ADVANCED PRACTICAL COURSE

Microchannel Plate Detectors

Experiment Leads:

Lauro CONTI & Sebastian DIEBOLD

Institut für Astronomie und Astrophysik
Kepler Center for Astro and Particle Physics
Eberhard Karls Universität Tübingen
Sand 1, 72076 Tübingen

Last edited: 26th March 2026

Contents

Acknowledgements

We gratefully acknowledge Dr. Jürgen Barnstedt for his invaluable efforts in designing, building, and maintaining the detector system used in this laboratory experiment. The experiment and these instructions are based extensively on his foundational work. References to Dr. Barnstedt's work are provided to give due credit to his contributions. As we explore the intricacies of MCP technology, we honor his legacy by aiming to provide students with a clear and thorough introduction to the field.

This laboratory manual has been developed and refined by several contributors. The following table outlines the major revisions and technical contributions:

Version	Contributor	Nature of Contribution
1.0	Jürgen Barnstedt	Initial development of the experiment and scientific content.
1.1	Sebastian Diebold & Tim Wildfang	Content updates and implementation of the LaTeX framework.
1.2	Lauro Conti	Scientific updates, structural refinement, and modernization.

1 Introduction

1.1 Historical background

Microchannel Plate (MCP) Detectors were built since the early 1980s in the former Astronomical Institute Tübingen (AIT), which is now the section Astronomy of the Institute for Astronomy and Astrophysics. These detectors are photon counting and imaging detectors for ultraviolet light. Later these detectors were built into encapsulated glass tubes together with a photocathode for visible light. For this optical detector system a fast readout electronics was developed (Digital Position Analyser, DPA), which was connected to a PDP11 computer for data acquisition. This camera system was used for observations at large telescopes, amongst others in Asiago (Italy), on Calar Alto (Spain), and at the European Southern Observatory (ESO) in Chile.

In the mid 1980s the space telescope *ORFEUS* (**O**rbiting and **r**etrievable **F**ar- and **E**xtreme-**U**ltraviolet-**S**pectrometer) was established as project and finally realized. AIT had the scientific project management and contributed with own hardware: The MCP detectors for the Echelle spectrometer were developed and built at AIT, as well as the corresponding electronics and the onboard computer for instrument control and data acquisition. *ORFEUS* was mounted on the reusable German satellite platform *ASTRO-SPAS* (**S**huttle **Pa**llet **S**atellite), which was built by the former company MBB (now part of Astrium).

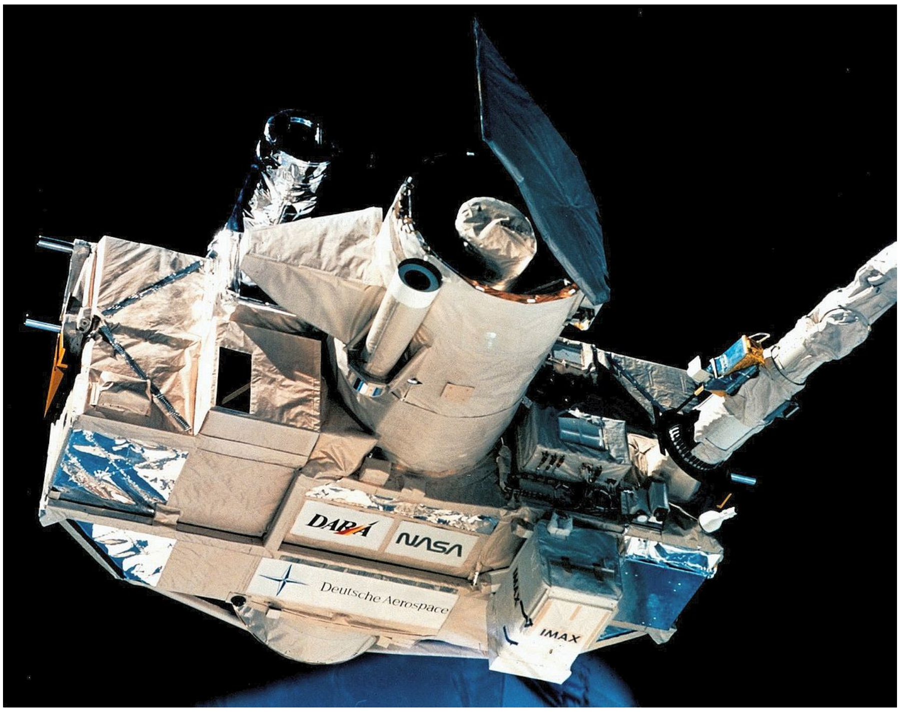

Figure 1.1. *ORFEUS* during the first mission 1993 (Image credit: NASA)

ORFEUS was flown on two space shuttle missions 1993 (4 days observation) and 1996 (14 days observation). Unfortunately, during the first mission no data could be gathered with the Echelle spectrometer due to a malfunctioning switchable mirror in the telescope. However, the mission overall was quite successful, as the second spectrometer, built by the University of California in Berkeley, took numerous measurements. The second *ORFEUS* mission was a major success, gathering a large amount of far ultraviolet spectra in the wavelength range 90 nm to 140 nm during its 14 days of free flight. With a total of 17.7 days in orbit, it set the record for the longest Spae Shuttle mission (STS-80)[1]. The instrument achieved a spectral resolution of $10,000$[2].

Shortly after the two flights it was clear that *ORFEUS* would not fly into space again. Meanwhile, the *ASTRO-SPAS* satellite is exhibited in the Deutsches Museum in München. The telescope structure, the primary mirror, and the Echelle spectrometer are at IAAT. The detectors are working and are used for research and teaching purposes. The UV detector group is actively developing advanced MCP detectors, as sealed-tube for the near UV as well as an open-face version for far and extreme UV.

In this experiment we will study the characteristics and applications of these microchannel plate detectors.

[1] More details about the ORFEUS project can be found on our website: https://uni-tuebingen.de/en/4221.

[2] The spectral resolving power is defined as $R = \lambda/\Delta\lambda$. A resolution of $10,000$ at 100 nm thus implies a minimum resolvable wavelength difference of $\Delta\lambda = 0.01$ nm.

Hints for the preparation

To simplify your preparation to this experiment we interspersed some exercises in the text of the theoretical introduction. You should have answered these questions **beforehand**, as these questions will be part of the oral examination before carrying out the experiment. The solutions will also be part of the protocol. This manual was kept quite detailed in order to give sufficient background information for this experiment. The following chapters are not essential for the understanding of the experiment and may be skipped in case of short preparation time: 1.2, 2.2.1, 2.3.3, 3.4, 3.5, 3.6. Additionally, the guidelines for the Advanced Labwork in Astronomy and Astrophysics have to be followed. While the laboratory documentation provides specific examples using Excel (e.g., CSV processing), you are encouraged to use any established computational tool or programming language (such as Python, or MATLAB) for your analysis and plotting. Regardless of the tool chosen, ensure that all scripts and derived parameters are documented transparently in the protocol.

1.2 Results of the Echelle spectrometer of the *ORFEUS II* mission

This section will show some of the most important results achieved with the Echelle spectrometer during the second *ORFEUS* mission. Fig. 1.2 shows an original measurement of the Echelle spectrometer, a spectrum of the white dwarf HD 93521. This image is not quadratic, as the data were recorded in X-direction (main dispersion of the spectrometer) with 1024 pixels, while in Y-direction (cross dispersion) only 512 pixels were recorded, which was sufficient to separate the individual spectral orders (numbered from 40 to 60 in this image). The wavelength range starts at about 90 nm (order 61, centre) and ends at about 140 nm (order 40, top left). An Echelle spectrometer comprises two different gratings. The high spectral resolution is produced by a Echelle grating, which operates in high spectral orders (here: orders 40 – 61). As these diffraction orders overlap each other, a second grating (cross disperser) is used to achieve dispersion with a low spectral resolution perpendicular to that of the Echelle grating. Thus the overlapping orders of the Echelle grating are arranged below each other on the detector, and the individual orders run slightly tilted across the image.

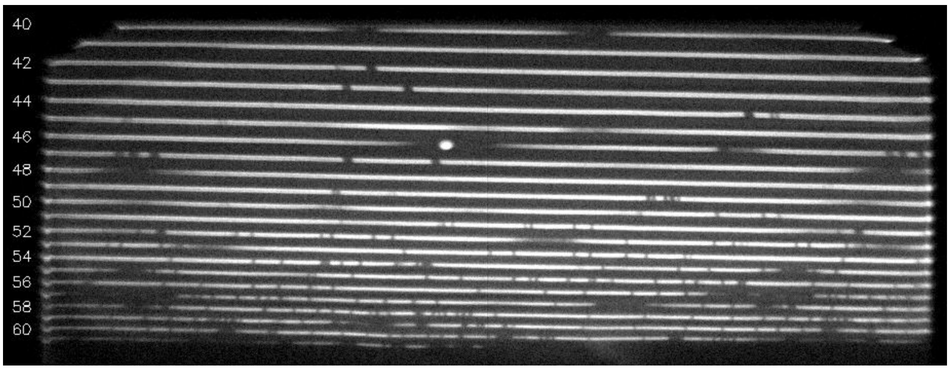

Figure 1.2. Echelle spectrum of the white dwarf HD 93521. Left hand the orders of the Echelle grating are shown, starting with order 40 at a wavelength of about 140 nm (top left)

The image shows already quite clearly some absorption lines as dark areas. You may also distinguish two different kinds of absorption lines: broad and narrow ones. The broad lines are broadened due to the Doppler Effect. They originate from hot gases and are therefore of stellar origin (stellar atmosphere). The narrow lines conversely originate from cold gas clouds, which are located somewhere in interstellar space between earth and the observed star. A closer look reveals that some of the narrow lines are double lines. These are Doppler shifted lines which means, that the light passed through two different gas clouds which move with different velocities relative to the earth. Fig. 1.3 shows a plot of a section of this spectrum with absolutely calibrated flux and wavelength scales together with many identified absorption lines. A total of more than 300 different absorption lines were identified (Barnstedt et al., 2000, [1]). Very remarkable is the multitude of nearly 200 absorption lines of molecular hydrogen H_2 in this spectrum, which originate from at least two different interstellar gas clouds. H_2 is observable only in this *ORFEUS* wavelength range. Even some stellar atmospheres contain molecular hydrogen H_2 and its ions H_2^+. These short living molecules form at high gas pressure and are called quasi molecules. With *ORFEUS* they could be measured for the first time in a wavelength range below 120 nm.

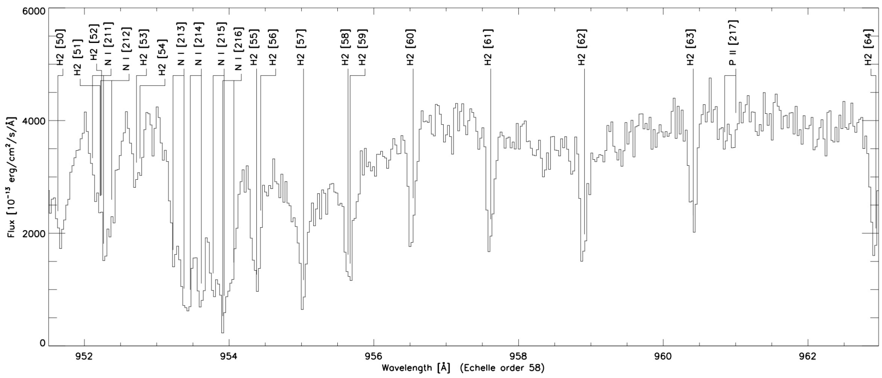

Figure 1.3. Section of the Echelle spectrum of the white dwarf HD 93521. The identified absorption lines are marked: H2 = molecular hydrogen, OI = neutral oxygen, NI = neutral nitrogen, PII = single ionised phosphorus, HI = neutral hydrogen (line of the Lyman series, Lyman-γ = 972.537 nm, stellar line). (Source: Barnstedt et al. 2000 [1])

Also in the spectra of stars of the two Magellanic Clouds cold H_2 could be detected. The absorbing gas clouds are high velocity clouds in the halo of our own galaxy and therefore they have nothing to do with the Magellanic Clouds. In one case even absorption lines of highly excited states were observed, which indicated an illumination of this gas cloud with UV light. Such high excitations were observed with *ORFEUS* for the first time. Besides hydrogen in some of the spectra also deuterium could be found. Deuterium was produced during the Big Bang and was dissipated later by stellar burning processes. Thus the amount of deuterium decreases during the development of the universe. With *ORFEUS* the abundance of interstellar deuterium in the direction of two stars could be determined – for the first time from the measurement of 5 or 6 absorption lines. This allowed for the estimation of the interstellar D/H

ratio. The values were within the range of previously known measurements. From spectra of the Large Magellanic Cloud a lower limit for the H_2/CO ratio could be estimated. CO is quite common in space and can also be observed at radio frequencies, in contrast to H_2. Therefore CO can be observed rather easily all over the space and it is assumed that H_2 occurs there, where also CO occurs. So a direct estimation of the H_2/CO ratio is important to deduce the amount of H_2 from CO measurements. By observation of emission lines of fivefold ionised oxygen (O VI, visible only in the *ORFEUS* wavelength range) of symbiotic stars it could directly be shown, that this radiation produces emission lines in the visible spectral range by Raman scattering. The oxygen emission lines are absorbed as hydrogen Lyman-α line and the excess energy is emitted as line in the visible range. This process was already known, but it was the first time, that it could directly be observed. In general by observation of O VI very hot gases of about 200 000 K can be detected. With *ORFEUS* this detection succeeded also for gas clouds in the halo of our galaxy. Finally for the first time it was possible to observe HD molecules in the Small Magellanic Cloud. A more detailed summary can be found on this web page (in German): http://www.uni-tuebingen.de/en/4319

2 Functional Principle of MCP Detectors

2.1 Introduction

Microchannel Plate (MCP) detectors are high-resolution, photon-counting imaging devices. They are designed to register individual incident photons, calculate their arrival coordinates, and store this spatial information for subsequent analysis.

The primary components of the detector used in this laboratory are:

- A **photocathode and MCP stack**. The photocathode converts incident UV photons into photoelectrons, while the MCP stack amplifies these electrons into a measurable charge cloud.
- A **readout anode**, such as the Wedge-and-Strip Anode (WSA) used in the ORFEUS mission. It collects the charge cloud such that the detector electronics can calculate its centroid, which is correlated to the position of the incident photon.

An MCP is a thin plate comprising millions of microscopic glass capillaries (channels) bundled together. In this experiment, the substrate of the plates is lead glass. The front and back surfaces are coated with a metallic layer to serve as electrodes. A high voltage (typically $\approx$ 1000 V per plate) is applied between these electrodes. This potential difference establishes a strong axial electric field within each channel.

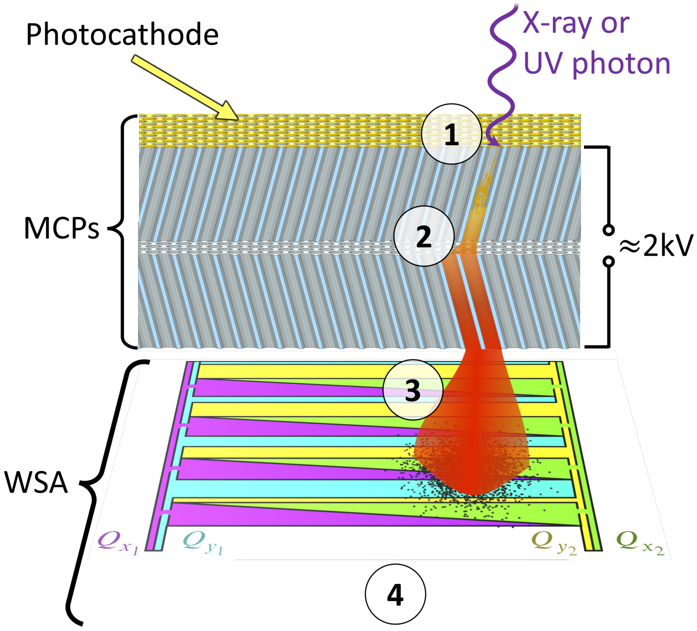

Figure 2.1. Functional principle of an MCP detector in chevron configuration with a Wedge-and-Strip anode. The numbered labels correspond to the steps described in the text.

Additionally, in some MCP detectors, a photocathode is deposited on the front surface of the first MCP. This is a thin film with high quantum efficiency in the energy range of interest, i.e. a high probability of releasing a photoelectron when hit by a photon. The detection chain used to determine the x, y, and time coordinates of incident photons is summarised below (the numbered steps correspond to the labels in Fig. 2.1):

1. **Photoemission:** Under vacuum, an incident UV photon strikes the photocathode near or inside a specific channel, releasing a primary photoelectron via the external photoelectric effect.

2. **Electron Multiplication:** The electric field accelerates this electron towards the rear (output) of the channel. Upon colliding with the wall, it triggers the emission of multiple secondary electrons. This process repeats several times along the channel length, creating an electron avalanche. For a single incident photon, an electron cloud containing about 10^4 electrons (for the ORFEUS detector) exits the rear of the MCP. This amplification factor is called the gain. Several MCPs can be stacked to achieve higher gains.

3. **Anode Impact:** The electron cloud is accelerated towards the readout anode. In the case of the **Wedge-and-Strip Anode (WSA)**, the cloud is distributed across the specific electrode geometries (wedges and strips).

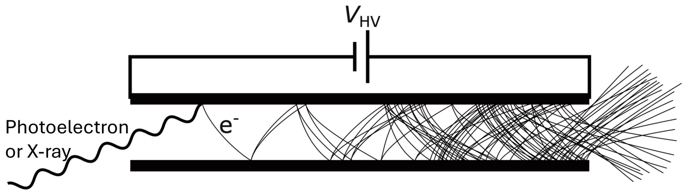

Figure 2.2. Electron multiplier channel. Adapted from [4].

4. **Charge Amplification:** The induced charges $Q_{x_1}, Q_{x_2}, Q_{y_1}$ and Q_{y_2} are amplified by charge-shaping amplifiers and converted into bipolar voltage pulses. The pulse amplitudes are digitised by Analogue-to-Digital Converters (ADCs).

5. **Position Centroiding:** For the WSA used here, the ratio of charges collected by the four electrodes is used to calculate the centroid of the charge cloud. This centroid corresponds to the original x, y coordinates of the incident photon. The final spatial coordinates are stored by the data acquisition system.

6. **Timing:** The arrival time of the photon is derived from the timing of the detector pulse in the associated electronics. In accelerator experiments, MCP-based detectors can achieve time resolutions in the picosecond regime [3]. In astronomy, timing information on the order of milliseconds is often sufficient to correct for pointing jitter.

In the ORFEUS detector this process can occur up to 100,000 times per second. By storing the position of each detected photon in a bitmap, a two-dimensional image of the observed source is reconstructed.

2.2 Microchannel plates and electron multiplier channels

The following sections cover function and characteristics of MCPs and electron multiplier channels.

2.2.1 Electron multiplier channels

MCP channels amplify electrons through an avalanche process. A primary electron entering the channel strikes the channel wall and releases secondary electrons. These electrons are accelerated by the electric field inside the channel and strike the wall again, producing further secondary electrons. Repeating this process along the channel length leads to an electron avalanche and forms an electron cloud that is detected as a charge pulse at the anode.

Typical gains of a single MCP channel are on the order of 10^3–10^4. As the electron avalanche grows, space-charge effects and the depletion of charge in the channel wall limit the multiplication process. When too many electrons are produced within a short time, the local electric field is reduced and the channel temporarily reaches saturation.

So-called *channeltrons* operate on a similar principle. They consist of a single curved electron multiplier channel with a funnel-shaped entrance that improves the collection efficiency for incoming electrons. The curved geometry helps suppress ion feedback by preventing positive ions from travelling back to the entrance of the channel.

2.2.2 MCP configurations

Ion feedback arises from the ionisation of residual gas atoms within the channels. During the electron avalanche, energetic electrons can ionise these atoms, producing positively charged ions. These ions are accelerated towards the entrance of the channel but move more slowly due to their larger mass. When they strike the channel walls, they can release additional electrons and produce delayed pulses, known as *ion feedback*. This effect can degrade the detector performance and may even lead to unstable operation.

Several design approaches are used to suppress ion feedback and increase the achievable gain of MCP detectors. One method is the use of curved channels, which prevent ions from travelling directly back to the entrance of the channel. More commonly, several MCP plates are stacked to increase the gain while simultaneously reducing ion feedback.
In such stacks, the channels of each MCP are typically tilted by about 10° with respect to the MCP surface normal. Successive plates are rotated such that their channel bias angles point in opposite directions. Two MCPs in this arrangement form a *chevron configuration*, while three plates form a *Z configuration* (Fig. 2.3).
A single MCP plate typically provides a gain of about 10^3–10^4. By stacking multiple plates, significantly higher gains can be achieved. Chevron configurations typically reach gains of 10^6–10^7, while Z-stack configurations can reach gains above 10^7 before saturation occurs. The angled arrangement of the channels also strongly suppresses ion feedback.

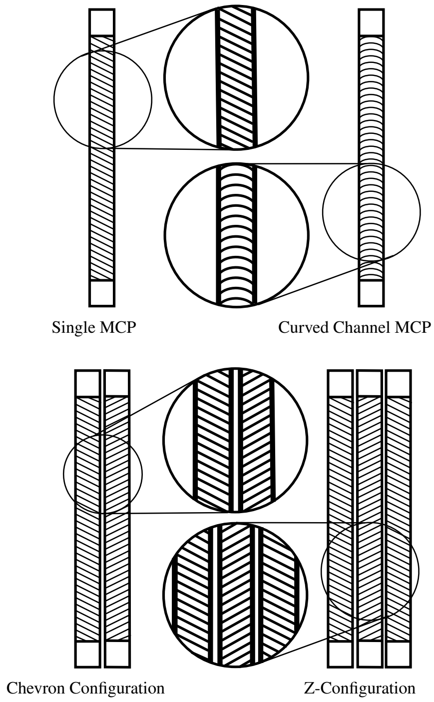

Figure 2.3. MCP configurations. Credit: T. Wildfang.

> **Exercise 1:**
> *Give two reasons for the fact, that MCPs can be operated only under vacuum. What would happen, if you would try to operate a MCP under atmospheric pressure?*

2.2.3 Gain and pulse height distribution

The gain of an MCP is an important parameter describing its amplification factor, i.e. the average number of electrons leaving the channel per primary electron entering the channel. The gain of a single MCP is mainly determined by the dimensionless channel length-to-diameter ratio l/d. It is usually in the range of 40 : 1 to 60 : 1, although higher ratios are also available [5]. A larger l/d ratio generally allows more collisions of electrons with the channel wall and therefore a higher gain.

Figure 2.4 shows the typical gain dependence on the applied voltage for the three common MCP configurations. The gain of an MCP is not exactly the same for every detected event, but shows a statistical variation from pulse to pulse.

If the charge deposited on the anode is measured for many individual events and the number of events is plotted as a function of pulse height, the resulting distribution is called the pulse height distribution. The inset plots in Fig. 2.4 show typical pulse height distributions for different MCP configurations. To distinguish real photon-induced events from the readout noise of the electronic system, a threshold is set in the signal processing chain. Only events above this threshold are accepted as valid detections. For a single MCP, the pulse height distribution is exponential, i.e. many events produce only a small charge, which makes it difficult to distinguish real photon events from electronic noise. This illustrates why configurations with at least two MCPs are required for photon-counting operation.

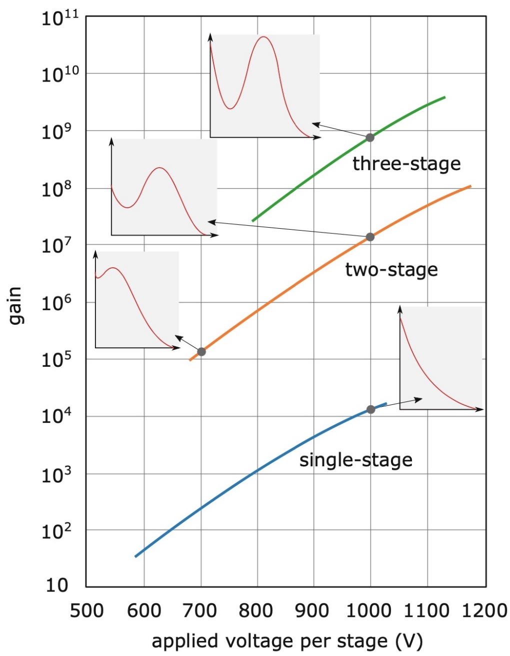

Figure 2.4. Typical gain dependence on the applied voltage for a single-stage MCP, a stack of two MCPs (*chevron stack*), and a stack of three MCPs (*Z stack*). The inset plots show the corresponding pulse height distributions at selected points on the gain curves, plotted as probability versus number of electrons per event. Adapted from [4].

2.2.4 Sensitivity

MCPs are sensitive to ionising radiation because particles or photons that deposit their energy close to the channel wall can release secondary electrons, which then enter the multiplication process. Only secondary electrons generated within about 20 nm of the channel wall surface can escape into the channel.

[3] FWHM stands for *full width at half maximum* and describes the width of a distribution at half of its maximum value.

Table 2.1. Typical performance parameters of different MCP configurations.

Configuration	Typical operating voltage (V)	Gain	Pulse height distribution
Single MCP	1000	10^3–10^4	exponential
Curved channel	2400	10^5–10^6	50% FWHM[3]
Chevron configuration	2000	10^6–10^7	120% FWHM
Z configuration	3000	10^7–10^8	80% FWHM

Table 2.2. Important photocathode materials [9]

Material	Long-wavelength limit (nm)
potassium bromide (KBr)	155
caesium iodide (CsI)	200
rubidium telluride (Rb_2Te)	300
caesium telluride (Cs_2Te)	350

The penetration depth of ultraviolet radiation (with energies above 8 eV), soft X-rays, electrons, and ions lies within this range.

For ultraviolet radiation, the long-wavelength limit of a bare MCP is about 150 nm (about 8 eV). At longer wavelengths, the sensitivity decreases rapidly. This makes MCPs naturally *solar blind*, which is an important property for space-based ultraviolet and X-ray detectors such as *ORFEUS*. For X-rays, the high-energy limit is about 0.1 nm (12.4 keV), because more energetic photons penetrate too deeply into the material and therefore rarely release secondary electrons that can escape into the channel.

To extend the UV sensitivity towards longer wavelengths, photocathodes can be deposited directly on the MCP surface. These materials absorb incoming photons, exciting a valence-band electron into the conduction band, which can then be emitted into the channel with high probability. Important examples are listed in Table 2.2. The choice of photocathode is a trade-off between sensitivity and chemical stability: materials with sensitivity at longer wavelengths are generally more sensitive to air exposure[4].

In addition, the collection efficiency can be increased by applying a weak electric field in front of the MCP. This field guides electrons released between the channels back into the pores, where they can still trigger an avalanche. In the *ORFEUS* detector, this was achieved by a mesh placed in front of the MCP. Although the mesh blocks about 10% of the incident photons, the improved electron collection results in a net sensitivity gain of about 20%.

2.2.5 Dark current

Even an MCP in complete darkness will produce pulses. This dark count rate is typically 0.2–1 counts s^{-1} cm^{-2}. About 90% of this dark current is caused by radioactive decay of components of the MCP glass (β decay of ^{40}K, half-life 1.28×10^9 years; [5]).

[4]This is because elements such as Cs and Rb, which must be used due to their low electron affinity, react heavily with oxygen and water.

Since these events originate not only at the entrance but at arbitrary positions within a channel, the resulting pulse height distribution has no pronounced maximum and instead shows a roughly exponential behaviour.

2.2.6 The MCPs of the ORFEUS detector

The MCPs used in the ORFEUS II detector are custom-made devices manufactured by Hamamatsu Photonics. The detector uses three MCPs stacked in a Z configuration, as introduced in the previous section. This configuration provides a total gain of about 10^7 to 10^8 electrons per detected photon.

The first two MCPs have a thickness of 1.0 mm, while the third MCP has a thickness of 0.6 mm. The plates have a diameter of 60 mm. The channel diameter is 12 µm with a centre-to-centre spacing of 15 µm (see also Exercise 2). For an MCP thickness of 1 mm, which corresponds to the channel length, this results in a length-to-diameter ratio of approximately 80:1.

The first MCP is coated with a KBr photocathode to enhance the detector sensitivity in the ultraviolet. A specially shaped electrode on the rear side of this MCP restricts the active detector area to 40 x 40 mm^2. This defines the field of view of the detector and matches the sensitive area of the readout anode (Fig. 2.5). A particular feature of the ORFEUS detector is that the three MCPs are mounted electrically isolated from each other with a spacing of about 0.3 mm. This allows each MCP to be supplied with an independent high voltage and also makes it possible to apply an additional acceleration voltage between the plates. The overall gain of the detector is mainly adjusted via the voltage applied to the third MCP.

In front of the MCP stack, at a distance of about 1 cm, a mesh biased to 500 V is installed. This mesh creates an electric field of approximately 50 $\frac{\mathrm{V}}{\mathrm{mm}}$ in front of the photocathode. The field redirects photoelectrons generated on the surface between the channel openings back into the channels, increasing the collection efficiency. Although the mesh blocks about 10% of the incoming photons, the improved electron collection results in a net sensitivity gain of ≈ 20%.

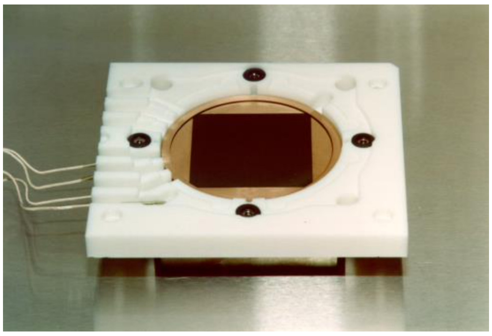

Figure 2.5. ORFEUS detector: view of the rear electrode of the first MCP that defines the active image area of the detector.

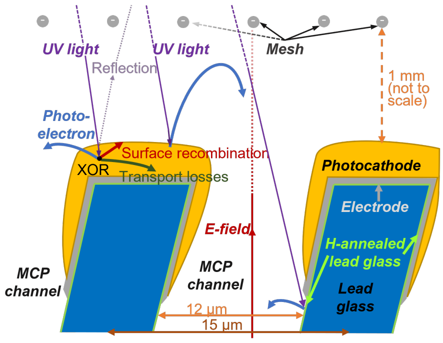

Figure 2.6. Summary of the geometry of a single channel, its materials, the absorption of incident UV photons and the release of the first electron.

Exercise 2:
Why are the three MCPs of the ORFEUS detector mounted electrically isolated from each other and supplied with separate high voltages? Give two advantages of this design for detector operation and explain why the detector gain is mainly adjusted via the voltage of the third MCP.

2.3 The anode

2.3.1 Introduction

The anode is located behind the MCPs. It serves as the collecting electrode for the electrons emerging from the MCP stack. The purpose of the anode is to encode the incident charge distribution in such a way that the position coordinates of the photon that triggered the charge pulse can be determined.

The Wedge-and-Strip Anode (WSA), originally developed by H. O. Anger (Martin et al., 1981, [7]), is based on the principle of charge division. This allows the position coordinates to be calculated from the ratios of the collected charges.

The distance between the MCPs and the anode is about 7 mm. A very homogeneous electric field is present between the MCPs and the anode, accelerating the electrons towards the WSA. Owing to the relatively large distance between the MCPs and the anode, the electron cloud expands during its flight. When it reaches the anode, the diameter of the charge cloud is typically a few millimetres.

2.3.2 The principle of the Wedge-and-Strip Anode

A Wedge-and-Strip Anode (WSA) consists of a gold layer deposited on a quartz substrate, into which a periodic structure of four different interleaved electrodes is etched. Two of these electrodes form a pair of complementary wedges, while the other two form a pair of complementary strips. The total width of each pair is constant, but the ratio of their widths varies across the anode. Figure 2.7 illustrates how the wedge electrodes encode the x position and the strip electrodes encode the y position.

For every electron cloud with a total charge Q above the trigger threshold, the charges collected on the corresponding electrode pairs are measured. The position is then calculated from the charge ratios

$$x = \frac{Q_{x_2}}{Q_{x_1} + Q_{x_2}}, \qquad y = \frac{Q_{y_2}}{Q_{y_1} + Q_{y_2}}. \tag{2.3.1}$$

These ratios map the detected position to a normalised coordinate between 0 and 1. For example, if the electron cloud is located very close to the left side of the anode, most of the charge is collected on the electrode Q_{x_1}, while Q_{x_2} becomes very small. In this case $x \approx 0$. Conversely, if the electron cloud is located near the right side of the detector, the charge is mainly collected on the electrode Q_{x_2} and the ratio approaches $x \approx 1$. An analogous relation holds for the y coordinate using the strip electrodes Q_{y_1} and Q_{y_2}.

A prerequisite for the anode to encode the position linearly is that the width of the electron cloud is approximately twice the period width of the anode structure. In this case, the cloud covers several electrode elements, so that the position can be derived reliably from the charge ratios. This is achieved by choosing the appropriate distance and electric field strength between the MCP and the anode. If the electron cloud is too small, periodic distortions appear in the recorded image. If it is too large, distortions increase in the border region of the image.

Such distortions in the border region cannot be avoided completely, since they are caused by the finite width of the electron cloud. In the *ORFEUS* detector, they are reduced by making the linear dimensions of the active anode area about 10% larger than those of the active detector image field. In addition, distortions caused by the width of the electron cloud can be minimised by extending the anode structure beyond the active area while keeping its geometrical parameters constant.

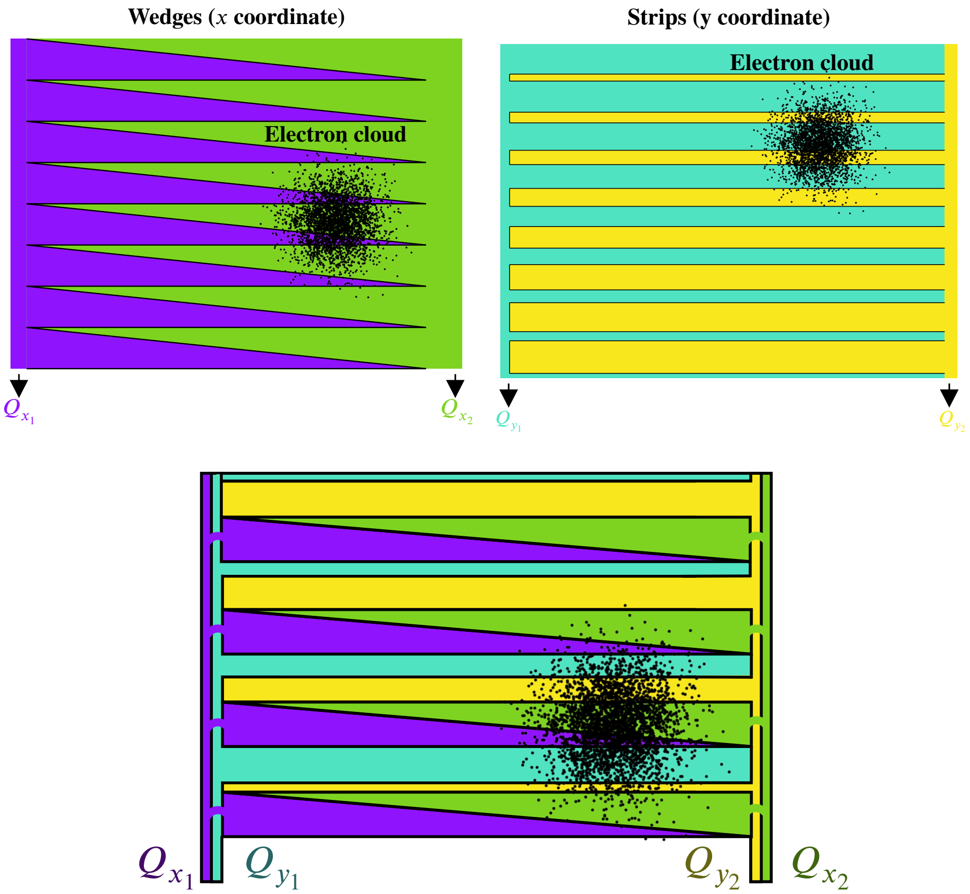

Figure 2.7. Principle of a Wedge-and-Strip Anode. The position coordinates (x, y) are calculated from the ratios of the collected charges Q_{x_1}, Q_{x_2}, Q_{y_1}, and Q_{y_2}.

Table 2.3. Technical data of the anode of the ORFEUS detector

Substrate	Quarz (Suprasil)
Size (length × width × thickness)	70 mm × 70 mm × 5 mm
Active area	44 mm × 44 mm
Width of passive area	7 mm
Period width (2 wedges + 2 strips)	1 mm
Distance between electrodes	20 μm
Conducting material	2 μm (Gold)

Exercise 3:
For good imaging performance, it is important to keep the capacitance between the four electrodes as small as possible. Why is a quartz substrate preferable to an ordinary glass substrate for the anode? (Quartz of the trademark Suprasil was used.)

2.3.3 The *ORFEUS* anode

Table 2.3 shows the technical data of the anode of the *ORFEUS* detector. This anode was manufactured by the company Heidenhain GmbH according to our specifications. Fig. 2.8 shows the *ORFEUS* anode in its mounting. The four electrical connections were glued with an electrically conductive adhesive onto the gold coating.

The *ORFEUS* anode comprises two additional electrodes on the back side of the quartz substrate with an area of 3.2 cm^2 each. They are located at two opposite corners of the active anode area. They form a capacitance with the anode so that rectangular test pulses could be coupled onto the anode by these electrodes. The falling edge of such pulses simulates an impinging electron cloud while the rising edge produces inverted pulses which are suppressed from being evaluated by the electronics. The test pulse electronics can selectively produce pulses on one of the two electrodes (bottom left LU = *links unten*, or top right RO = *rechts oben*) with 3 different pulse heights.

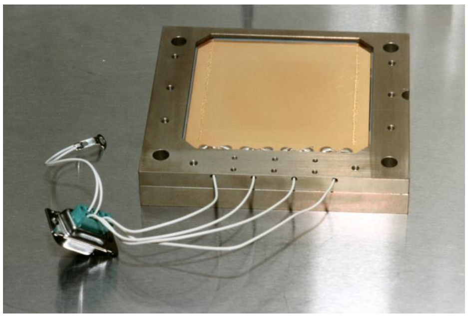

Figure 2.8. Wedge-and-strip-anode of the ORFEUS detector.

Exercise 4:
Calculate the capacitance of a test pulse electrode with respect to the anode (thickness of the anode: see Table 2.3). What voltage must a test pulse have to simulate a charge cloud with 10^7 *electrons?*

2.4 Readout electronics

The readout electronics register the charge pulses from the anode and calculate the position of the centroid of the charge cloud from the ratios of the collected charges. This position is then stored as the position of the incoming event. The electronics also convert the analogue detector signals into digital data. These data are processed by the Digital Position Analyser (DPA), which digitises the pulses and calculates the event position digitally. The resulting data are finally transferred to a computer.

2.4.1 Theory of operational amplifiers

The triangular symbol in Fig. 2.9 represents an operational amplifier (op-amp). An op-amp is a standard electronic component and is available in many different designs, optimised for a wide range of applications. However, the basic operating principle is simple.
An op-amp has two inputs ("+": non-inverting input and "-": inverting input) and one output. It amplifies the voltage difference between its two inputs by a very large factor. In most practical circuits, the output is fed back to the inverting input. This feedback causes the op-amp to adjust its output such that the voltage difference between the two inputs becomes very small. If the non-inverting input (+) is connected to ground, the inverting input (–) is therefore held at virtually ground potential.

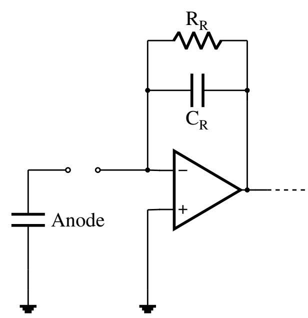

Figure 2.9. Principle of the operational amplifier. Credit: T. Wildfang.

2.4.2 Charge amplifiers

Charge amplifiers, which can be described as integrators, operate on this principle (Tietze/Schenk, Chapter 12.4; [8]). Figure 2.9 shows the basic circuit of a charge amplifier. The anode acts as a capacitance that collects the charge of an incoming pulse. If the anode were electrically isolated, the voltage across this capacitance would increase instantaneously when charge is deposited on it. In that case, the anode voltage U_{x_1} produced by a charge Q_{x_1} deposited on one wedge of the anode with capacitance C_{x_1} would be

$$U_{x_1} = \frac{Q_{x_1}}{C_{x_1}} . \tag{2.4.1}$$

In the actual charge amplifier, however, the anode is connected to the input of an operational amplifier. The input stage is configured as an integrator with a feedback capacitance C_R (the feedback resistor R_R will be neglected at first). As explained previously, the operational amplifier adjusts its output such that the voltage difference between its two inputs is approximately zero. Since the non-inverting input is connected to ground, the inverting input is therefore held at virtually 0 V. If a charge Q_{x_1} is deposited on the anode, a voltage step U_a appears at the output:

$$U_a = -\frac{Q_{x_1}}{C_R} \tag{2.4.2}$$

In simple terms, the deposited charge Q_{x_1} is transferred from the anode to the feedback capacitance C_R. The charge-to-voltage conversion of the amplifier is therefore only determined by the feedback capacitance C_R and deposited charge Q_{x_1}.

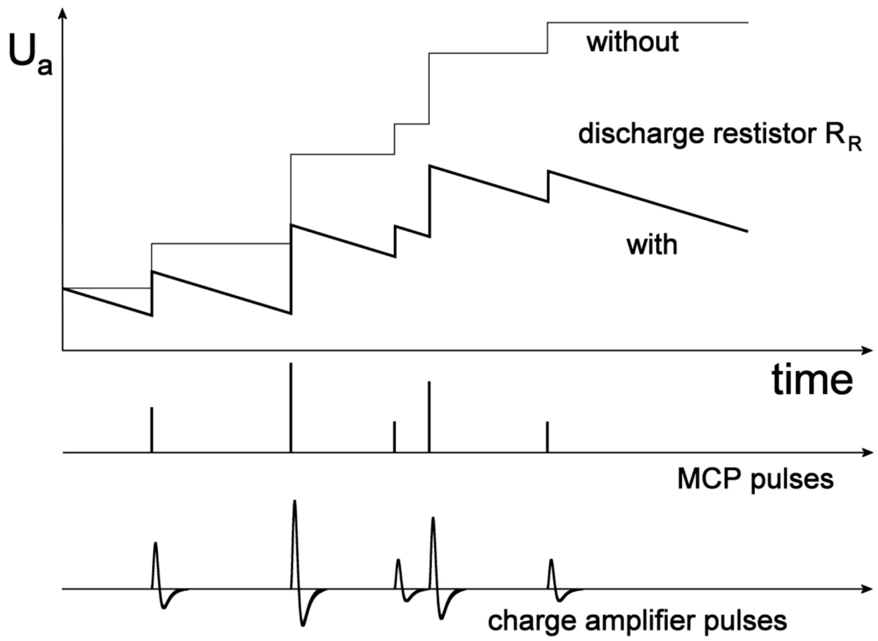

Figure 2.10. Principle of charge amplification: At the output of the integrator stage the incoming MCP pulses produce a voltage U_a which rises in steps for each pulse. Without feedback resistor R_R, which discharges the capacitor C_R, the output would result in an ever increasing voltage until the maximum voltage would be achieved. With discharge resistor the output voltage results in a saw tooth like course (the linear decline is the beginning of an exponential discharge curve). The information about the amount of charge is stored in the voltage steps. To be able to process this information in a more simple way, a filter stage is added to the charge amplifiers, which produce the bipolar pulses shown at the bottom (see also Fig. 2.12). The amounts of charge can now be evaluated from the peak voltages of the bipolar pulses.

The entrance stage is named integrator, as the output voltage is proportional to the time integral of the incoming current. In other words, the output voltage is proportional to the sum of the incoming charges. Without further measures the output voltage would increase until it is clipped by the supply voltage (Fig. 2.10). To avoid this, the feedback capacitance must be discharged slowly to bring the output voltage back to 0 V. This is the task of the feedback resistor R_R. R_R has to be chosen large enough, that U_a will not change within the time span that the electronics needs to register a pulse. On the other hand R_R has to be chosen small enough that the output voltage U_a will not be clipped at the highest expected pulse rates. The timing course of the output voltage U_a is such that a voltage step occurs at each impinging charge pulse which is followed by an exponential decay. The voltage will not drop to 0 V until the next pulse occurs, depending on the time when the next pulse arrives.

Exercise 5:

Estimate from Eq. 2.4.2 the formula for the charge amplification of the entrance stage (1. operational amplifier) of the charge amplifier shown in Fig. 2.9 in (Volt/Coulomb). Calculate the output voltage of this integrator stage for a feedback capacitance C_R = 3 pF and an impinging charge of 10^7 electrons.

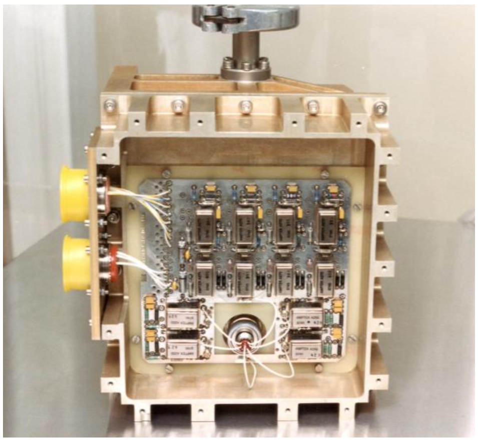

Figure 2.11. View of the charge amplifiers of the *ORFEUS* detector.

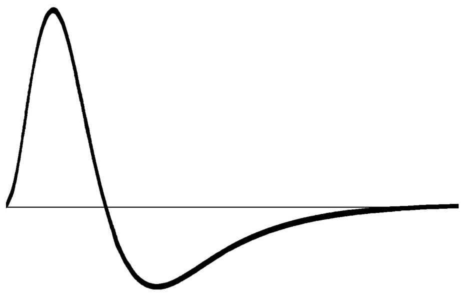

Figure 2.12. Form of the output pulse after the filter stage: Maximum at 1.1 μs, zero crossing at 2.3 μs. Time span shown: 10 μs.

2.4.3 Pulse shaping and transmission

The information required to register a photon event is initially contained in the voltage step at the output of the integrator stage. However, such a very short step on top of a slowly decaying baseline cannot be processed reliably by the following electronics. For this reason, the charge amplifiers located directly in the detector head contain an additional filter stage, which converts the voltage step into a well-defined bipolar pulse (Fig. 2.12).

These shaped pulses have two important advantages. First, they exhibit a pronounced maximum whose height is proportional to the deposited charge. This provides a well-defined quantity that can be digitised accurately by the ADC in the Digital Position Analyser (DPA). Second, the pulse returns to a stable zero level within a few microseconds, so that consecutive events can be separated more easily.

After amplification and pulse shaping in the detector head, the signals are transmitted over a relatively long distance to the DPA. For this purpose, capacitive coupling is used. This means that the signal is passed through a capacitor, which transmits only the time-dependent part of the signal while blocking constant voltage offsets (the DC component). Such coupling is particularly useful for long cables, because it prevents slow baseline shifts from being interpreted as real detector signals.

The bipolar pulse shape is especially well suited for capacitive coupling. Since the positive and negative pulse areas are equal, the average pulse voltage is zero. As a result, the baseline remains stable even when the count rate changes.

2.4.4 Digital Position Analyser

For every photon event, the charge amplifiers in the detector head send four voltage pulses to the analyser electronics. In the *ORFEUS* flight electronics, the analyser electronics determined the event positions, while an onboard computer performed the data acquisition. Both systems were developed at IAAT.

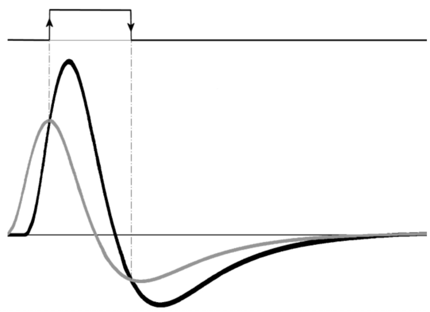

Figure 2.13. Determination of the signal maximum: an attenuated summed pulse (grey) and a delayed summed pulse (black) are fed into the two inputs of a comparator. The upper curve shows the output signal of the comparator.

In the present experiment, the Digital Position Analyser (DPA), originally built for an optical MCP detector, performs the following tasks:

- Pulse recognition
- Digitisation of the maximum values of the four voltage pulses (X_1, X_2, Y_1, Y_2) with 12-bit resolution
- Calculation of the sums $\sum X_i$ and $\sum Y_i$
- Calculation of the normalised position coordinates with 12-bit resolution:

$$x = \frac{X_2}{\sum X_i}, \qquad y = \frac{Y_2}{\sum Y_i}$$

- Calculation of the pulse height

$$Z = \sum X_i + \sum Y_i$$

- Acquisition of the arrival time of each event
- Transmission of the data to the computer

The pulse processing is controlled by electronic circuitry using the sum of the four charge-amplifier signals. A key task is the determination of the pulse maxima for digitisation. For this purpose, the summed signal is split into an attenuated branch (grey) and a delayed branch (black), which are fed into the two inputs of a comparator. A comparator is an electronic component that switches its output as soon as one input voltage becomes larger than the other. The attenuation is adjusted such that the delayed pulse crosses the attenuated pulse at its maximum, thereby triggering the analogue-to-digital converter at the correct time. In this way, the pulse maximum can be determined largely independently of the pulse height. Two additional comparators define the lower and upper discriminator thresholds, preventing the acceptance of pulses that are too weak or saturated. Figure 2.14 shows the front view of the DPA.

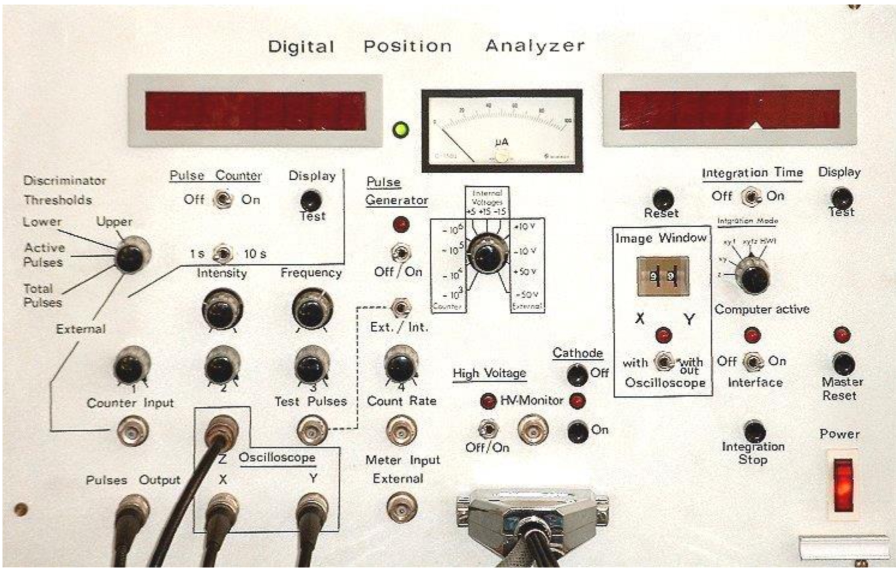

Figure 2.14. Front view of the DPA.

2.4.5 Data acquisition with the computer

A PC running the Windows operating system is used for data acquisition. This computer has two interfaces: a multifunction interface with analogue and digital inputs and outputs for controlling the detector and the high-voltage supply, and a fast 32-bit parallel interface for acquiring the detector data. Software is available both for controlling the high voltage and the test pulses and for data acquisition. The data acquisition can be operated in several modes:

- Image integration (x, y): recording of the coordinates with 10-bit resolution (image size 1024×1024 pixels)
- Integration of a pulse height distribution (Z)
- Integration of an image and a gain map (x, y, Z)
- Serial recording of all events, including the arrival time of each photon with microsecond resolution (x, y, Z, t)

2.5 Characteristics of the detector electronics

This chapter deals with those imaging properties of the detector system that are determined by the electronics. These include the noise of the charge amplifiers, unequal gain factors of the four charge amplifiers, and capacitive crosstalk between the four anode electrodes.

2.5.1 Noise

Since the position of a photon is calculated independently for each axis from two charge-amplifier signals, the noise in these signals has a direct influence on the spatial resolution of the detector. Electronic noise broadens the reconstructed position distribution and therefore degrades the sharpness of the recorded image. The noise can be described by a Gaussian distribution of the measured voltage around a mean value, with standard deviation σ_U. If a value x (analogous for y) is calculated from the voltages U_1 and U_2 as

$$x = \frac{U_1}{U_1 + U_2},$$

where the voltages U_1 and U_2 are superposed with noise of standard deviation σ_U, it can be shown (Knapp, 1978; [6]) that x is also Gaussian-distributed around a mean value. The standard deviation of x is then given by

$$\sigma_x = \frac{\sigma_U}{U_1 + U_2}\sqrt{2x^2 - 2x + 1}\,. \tag{2.5.1}$$

If many photons from an ideal point source are recorded, the reconstructed positions on the detector form a small spot with a finite width because of electronic noise, known as the point spread function[5]. If this spot is analysed only along the x direction, the spread of the measured x positions is described by σ_x. The expression $\sqrt{2x^2 - 2x + 1}$ becomes unity for $x = 0$ and $x = 1$ (i.e. at the border of the anode), while for $x = 0.5$ (i.e. in the middle of the anode) it reaches a minimum value of $1/\sqrt{2} = 0.71$.

For describing the resolution, it is more useful to use the full width at half maximum (FWHM) than the standard deviation σ:

$$\text{FWHM} = \sigma \cdot 2\sqrt{2 \ln 2} = 2.35 \cdot \sigma \tag{2.5.2}$$

[5] The point spread function describes how an ideal point source appears on the detector. Instead of a single point, one measures a small spot with a finite width.

The FWHM can be regarded as the resolution limit, i.e. the smallest distance at which two ideal point sources can still be distinguished. The FWHM in x-direction is therefore the distance that a line pair[6] in x-direction must be separated to be distinguished (ideally, i.e. if there was only noise). The resolution in line pairs per unit length is therefore given by 1/FWHM.

2.5.2 Partition noise

The electron cloud impinging on the anode comprises a finite number of electrons. These electrons are distributed among the four electrodes. This partitioning results in statistical fluctuations in the number of electrons arriving at each electrode. These fluctuations are referred to as *partition noise*. In the following, it is examined whether these fluctuations are relevant for the accuracy of the calculated position or can be neglected.

For simplicity, the position encoding in the two axes is assumed to be independent. The two wedge electrodes, or the two strip electrodes, each receive half of the total charge arriving at the anode. Consider the wedge electrodes, which encode the x direction. At position x (normalised, $0 \leqslant x \leqslant 1$), a charge cloud with total charge Q impinges on the anode. Both wedges together receive the charge $Q/2$ and the corresponding number of electrons $N/2$, with $N = Q/q$ and electron charge q. On average, wedge electrode 1 receives $N_1 = x \cdot N/2$ electrons and wedge electrode 2 receives $N_2 = (1 - x) \cdot N/2$ electrons.

Statistically, each of the $N/2$ electrons reaches electrode 1 with probability $p_1 = x$ and electrode 2 with probability $p_2 = 1 - x$. Such a situation, in which one event can result in one of two outcomes, is described by a binomial distribution (Weinzierl / Drosg, 1970; [10]):

$$P_{n,p}(k) = \binom{n}{k} \cdot p^k \cdot (1-p)^{n-k} \tag{2.5.3}$$

The distribution $P_{n,p}(k)$ describes the probability that, after n trials, exactly k successful events are registered, if the probability of a successful event is p. In the present case, the number of trials is $n = N/2$, i.e. the number of electrons impinging on the wedge electrodes. A successful event corresponds to the arrival of an electron at electrode 1, hence $p = p_1 = x$, and k is the number of electrons collected by electrode 1.

For the standard deviation σ of the values k around the mean value N_1, the following relation applies for a binomial distribution:

$$\sigma = \sqrt{p \cdot (1-p) \cdot n} = \sqrt{x \cdot (1-x) \cdot \frac{N}{2}} \tag{2.5.4}$$

The expression on the left-hand side gives the general form, while the right-hand side is obtained for the definitions introduced above.

σ becomes zero at the borders of the anode ($x = 0$ and $x = 1$), while it reaches its maximum at the centre ($x = 0.5$):

$$\sigma_{\max} = 0.5 \cdot \sqrt{N/2}.$$

To obtain the standard deviation of the relative position x ($0 \leqslant x \leqslant 1$), this value must be divided by the number of electrons $N/2$. In addition, Eq. 2.5.2 is used to convert the standard

[6] A line pair consists of two bright and one dark line.

deviation approximately into an FWHM. The following expression is therefore obtained for the FWHM of a point image in the centre of the anode broadened by partition noise:

$$\mathrm{FWHM}_{\mathrm{part}} = 2.35 \cdot \frac{1}{\sqrt{2N}} = 1.66 \cdot \frac{1}{\sqrt{N}} \tag{2.5.5}$$

Its inverse provides a measure of the spatial resolving power along one axis. This yields the following values: for $N = 10^6$, 600; for $N = 10^7$, 1900; and for $N = 10^8$, 6000. Partition noise therefore does not dominate the resolution of a detector with 1024 pixels per axis if more than about 10^7 electrons are present in each electron cloud.

2.5.3 Crosstalk

The electrodes of the Wedge-and-Strip Anode act as capacitances with respect to one another. The charge amplifiers have a finite input capacitance. Depending on the ratio of amplifier input capacitance to electrode capacitance, a fraction of the charge arriving at one electrode is coupled capacitively to the other electrodes. This effect is called *crosstalk*. In the following, its influence on the calculated position x' is examined.

First, consider the ideal coordinate in one axis, for example the x direction, which is calculated from the two wedge charges Q_{x_1} and Q_{x_2} (with total charge $Q_x = Q_{x_1} + Q_{x_2}$):

$$x = \frac{Q_{x_2}}{Q_{x_1} + Q_{x_2}} = \frac{Q_{x_2}}{Q_x} \tag{2.5.6}$$

The coordinate x can take values from 0 (left border of the anode) to 1 (right border of the anode). The measured voltages U_1 and U_2 are obtained with amplification factor v and crosstalk fraction b as

$$U_1 = v \cdot (Q_{x_1} + bQ_{x_2}), \qquad U_2 = v \cdot (Q_{x_2} + bQ_{x_1}).$$

Thus, the measured position (influenced by crosstalk) x_{ct} is

$$x_{ct} = \frac{U_2}{U_1 + U_2} = \frac{Q_{x_2} + bQ_{x_1}}{Q_{x_1} + bQ_{x_2} + Q_{x_2} + bQ_{x_1}} \tag{2.5.7}$$

If Eq. 2.5.6 is rearranged for Q_{x_2} and then substituted into Eq. 2.5.7, the total charge Q_x cancels and the following relation between the measured position x_{ct} and the true position x is obtained:

$$x_{ct} = \frac{x(1-b)+b}{1+b} = x\frac{1-b}{1+b} + \frac{b}{1+b} \tag{2.5.8}$$

As a consistency check:

$$\begin{aligned} x = 0&: \quad x_{ct} = b/(1+b) \\ x = 1/2&: \quad x_{ct} = 1/2 \\ x = 1&: \quad x_{ct} = 1 - b/(1+b) \end{aligned}$$

Thus, crosstalk causes the recorded image to shrink, because both borders are shifted towards the centre by the amount $b/(1+b)$. The distortion is therefore linear: positions near the centre remain almost unchanged, while positions near the borders are shifted most strongly inwards. This image shrinkage can be corrected to the first order by a linearity calibration, for example by imaging a grid on the detector and applying the corresponding correction in software.

2.5.4 Amplification differences

Accurate linear imaging requires the two charge amplifiers whose signals are used to calculate the position along a given axis to have exactly the same gain and the same temporal behaviour. This, in turn, requires the corresponding electronic components in the two circuits shown in Fig. 2.9 to have identical values. Since all electronic components exhibit a certain tolerance with respect to their nominal values, the actual values of many components must be measured and the best-matching pairs selected for the corresponding positions in the two charge amplifiers. In laboratory electronics, resistors can be adjusted using potentiometers. Capacitors can likewise be adjusted by means of trimmer capacitors. However, such options are not available for electronics intended for space applications, since potentiometers are not sufficiently shock-resistant. Instead, one or two additional adjustment resistors must be selected and fixed by soldering them into the circuit. In practice, this usually yields matching accuracies only at the level of a few per cent. Consequently, the gain factors are generally identical only within a few per cent. This leads to non-linearities in the imaging that must be taken into account during data reduction.

The effect of unequal gain factors on the measured position can be described analytically. The true position x is defined in Eq. 2.5.6. Ideal charge amplifiers produce voltage pulses U_1 and U_2 that are exactly proportional to Q_{x_1} and Q_{x_2}. In practice, however, the two gain factors differ slightly. We therefore assume

$$U_1 = v \cdot Q_{x_1} \qquad \text{and} \qquad U_2 = v \cdot (1 + a) \cdot Q_{x_2},$$

where a is a small correction term describing the gain mismatch and may also be negative. The electronics therefore calculate the position (influenced by amplification differences) x_{ad} as

$$x_{ad} = \frac{U_2}{U_1 + U_2} = \frac{Q_{x_2}(1 + a)}{Q_{x_1} + Q_{x_2}(1 + a)} \tag{2.5.9}$$

If Eq. 2.5.6 is rearranged for Q_{x_2} and substituted into Eq. 2.5.9, the total charge Q cancels, and the following relation between the measured position x_{ad} and the true position x is obtained:

$$x_{ad} = x\frac{1 + a}{1 + xa} \tag{2.5.10}$$

As a consistency check, the identity $x_{ad} = x$ is recovered for $a = 0$. In all other cases, the values at the borders remain unchanged: $x = 0$ gives $x_{ad} = 0$, and $x = 1$ gives $x_{ad} = 1$. The distortion therefore leaves the image borders fixed, while the image scale changes across the field and the central region is displaced. As in the case of crosstalk, this effect must be corrected during data reduction. It should be noted that crosstalk acts before the unequal gain factors enter the position calculation.

The derivative of x_{ad} with respect to x describes the local image scale, i.e. the number of pixels per unit length at the anode position x (if x_{ad} is given in pixels and x in physical anode coordinates):

$$\frac{dx_{ad}}{dx} = \frac{1 + a}{(1 + xa)^2} \tag{2.5.11}$$

Its reciprocal therefore gives the effective pixel size at the anode position x. A value of 1 corresponds to the nominal value, as is obtained, for example, when $a = 0$. There is always a position x at which the derivative is equal to 1, since at the two borders one value is larger than 1 and the other is smaller than 1.

Setting $dx_{ad}/dx = 1$ and solving for x gives

$$x = \frac{\sqrt{1+a}-1}{a} \approx \frac{1}{2} - \frac{1}{8}a \tag{2.5.12}$$

The approximation on the right-hand side is obtained by expanding the square root in a series up to the quadratic term. As expected, the nominal pixel size is obtained close to the centre of the image.

Exercise 6:
Derive Eq. 2.5.11 from Eq. 2.5.10.

2.5.5 Offset

As described in Sect. 2.4.3, the output pulses of the charge amplifiers are transmitted capacitively without shifting the zero level of the signal lines. However, such zero-level shifts may arise during the subsequent signal processing, in particular in the analogue-to-digital converters (ADCs). These shifts are referred to as offset voltages. For this reason, each ADC channel in the DPA contains a potentiometer that allows the offset voltage to be adjusted to zero.

The influence of such an offset error on the recorded image can be derived analytically. Assume that a constant offset voltage is present on the second signal channel, corresponding to an offset charge Q_{off}. With $U_1 = \nu \cdot Q_{x_1}$ and $U_2 = \nu \cdot (Q_{x_2} + Q_{\text{off}})$, the calculated position (influenced by an offset) x_{os} becomes

$$x_{os} = \frac{U_2}{U_1 + U_2} = \frac{Q_{x_2} + Q_{\text{off}}}{Q_{x_1} + Q_{x_2} + Q_{\text{off}}} \tag{2.5.13}$$

Using the same definitions of x and Q_x as in the previous sections, this expression can be rewritten as

$$x_{os} = x \frac{1}{1 + \frac{Q_{\text{off}}}{Q_x}} + \frac{Q_{\text{off}}}{Q + Q_{\text{off}}} \tag{2.5.14}$$

Assuming that $Q_{\text{off}} \ll Q_x$, the first fraction can be expanded to first order, while in the second fraction Q_{off} can be neglected with respect to Q_x:

$$x_{os} \approx x \left(1 - \frac{Q_{\text{off}}}{Q_x}\right) + \frac{Q_{\text{off}}}{Q_x} \tag{2.5.15}$$

Considering the limiting cases:

$$x = 0: \quad x_{os} = Q_{\text{off}}/Q_x$$
$$x = 1: \quad x_{os} = 1$$

Thus, no change occurs at the right border ($x = 1$), whereas the left border ($x = 0$) is shifted by the amount Q_{off}/Q_x. The magnitude of this shift therefore depends on the total charge and is largest for small pulses. The effect is strongest at the side of the image where the signal affected by the offset error (Q_{x_2} in this example) is small, since in that case the relative error Q_{off}/Q_{x_2} becomes particularly large. Offset errors are therefore especially critical for weak events, because they introduce a pulse-height-dependent position shift.

2.5.6 Dead time

The electronic effect of dead time influences the efficiency of the detector. Dead time denotes those time intervals during which the electronics is unable to process incoming pulses. This may be because it is still occupied with processing a previous event (e.g. during the analogue-to-digital conversion), or because a measurement at that instant would be distorted (e.g. during the undershoot of a pulse; see Fig. 2.12).

The DPA performs the analogue-to-digital conversion within 2 µs, which is significantly faster than the decay of the charge-amplifier pulses. The position calculation itself is also carried out very rapidly, taking only about 0.5 µs. The charge-amplifier pulses therefore represent the slowest element in the signal-processing chain. They require about 10 µs to 13 µs until the zero level is fully restored. Only after this time can a new pulse be processed reliably, since otherwise the signal would be distorted by an offset error.

To suppress signal processing during the undershoot of the charge-amplifier pulses, the control logic contains a monoflop that is triggered at the zero crossing of the pulses after about 2 µs. It inhibits pulse recognition for approximately 11 µs. Pulses arriving during this interval are therefore ignored. In addition, the monoflop is retriggered by newly arriving pulses, i.e. its active state is extended by a further 11 µs from that moment onwards. The total dead time associated with one pulse is therefore about 13 µs.

Pulses arriving within the first microsecond, i.e. before the maximum of the first pulse is reached, cannot be separated by the electronics. Such nearly simultaneous pulses are therefore processed as a single pulse. This effect is called *pile-up*. Since most of these double pulses are large enough to exceed the upper discriminator threshold, they are suppressed to a large extent.

The influence of dead time on the electronic efficiency of the system can be described statistically. The registered events in the detector are statistically independent of one another and can therefore be described by a Poisson distribution (Weinzierl / Drosg, 1970, [10]):

$$P_x = \frac{m^x e^{-m}}{x!} \tag{2.5.16}$$

This expression gives the probability of observing exactly x positive events if the mean value of the distribution is m. In the present case, positive events are the pulses occurring during the observation time t. For a mean count rate n_0, the mean value is given by

$$m = n_0 \cdot t \tag{2.5.17}$$

The probability that no event occurs during the measuring time t is therefore (with $0! = 1$):

$$P_0 = e^{-n_0 t} \tag{2.5.18}$$

The probability that a pulse occurs in the small time interval between t and $t + dt$ following t is exactly $n_0 \cdot dt$ (by definition of n_0 and for $dt \ll 1/n_0$). Since these probabilities are statistically independent, they can be multiplied to determine the probability that exactly one event occurs after time t within the interval dt:

$$dP_t = n_0 \cdot e^{-n_0 t} dt = e^{-n_0 t} d(n_0 t) \tag{2.5.19}$$

Consequently, short intervals between pulses occur with exponentially higher frequency. It is therefore fundamentally impossible to perform lossless measurements using electronics affected by dead time. Electronics with a dead time τ only register events if the interval from the preceding pulse exceeds τ. Integrating Equation 2.5.19 yields the probability of pulse intervals $t > \tau$:

$$P_{t>\tau} = \int_{t=\tau}^{\infty} dP_t = n_0 \int_{\tau}^{\infty} e^{-n_0 t} dt = e^{-n_0 \tau} \tag{2.5.20}$$

Since the average of n_0 pulses arriving per unit time are statistically independent, the number of events n registered by the electronics is given by:

$$n = n_0 \cdot e^{-n_0 \tau} \tag{2.5.21}$$

For very high pulse rates ($n_0 \to \infty$), n approaches zero, meaning practically all pulse intervals are shorter than the dead time τ. The curve defined by Eq. 2.5.21 thus exhibits a maximum. Differentiating Eq. 2.5.21 with respect to n_0 and determining the root yields the maximum at $n_0 = 1/\tau$. The maximum registrable event rate is therefore:

$$n_{\text{max}} = \frac{1}{\tau \cdot e} \tag{2.5.22}$$

For $\tau = 13\,\mu$s, the maximum registrable event rate is $n_{\text{max}} = 28,300\,\text{s}^{-1}$ at an incident pulse rate of $n_0 = 76,900\,\text{s}^{-1}$; the resulting efficiency is $1/e = 37\,\%$ (Fig. 2.15).

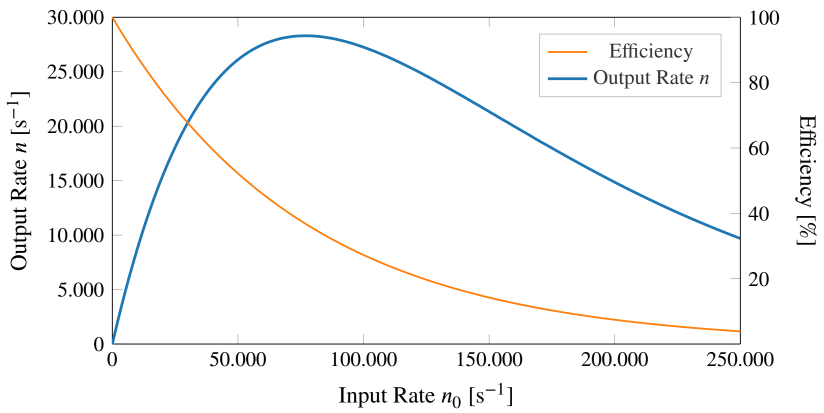

Figure 2.15. Output rate and efficiency for a dead time of $\tau = 13\,\mu$s.

To determine the actual pulse rate n_0 from a measured count rate n with a known dead time τ, the following approximation is typically used, as Equation 2.5.21 cannot be solved analytically for n_0:

$$n_0 \approx \frac{n}{1 - n \cdot \tau} \tag{2.5.23}$$

This correction is only applicable for count rates significantly lower than $1/\tau$. If $n_0 < 14\,\%$ of $1/\tau$ ($n < 12\,\%$), the error associated with this formula is less than 1 %. At $n_0 = 44\,\%$ of $1/\tau$ ($n = 28\,\%$), the error increases to 10 %.

A more accurate approximation can be derived by expanding the exponential function in Equation 2.5.21 into a power series. Considering the terms up to the quadratic term and solving for n_0 yields, after a lengthier calculation:

$$x_0 \approx \frac{1}{3}\left(2 + \sqrt[3]{x' + \sqrt{x'^2 + 8}} + \sqrt[3]{x' - \sqrt{x'^2 + 8}}\right) \tag{2.5.24}$$

Here, $x' = (27x - 10)$, where x and x_0 represent the normalized count rates: $x = n\tau$ and $x_0 = n_0\tau$. For $n_0 < 0.33/\tau$ ($n < 0.24/\tau$), this correction results in an error of $< 1\%$, and for $n_0 < 0.62/\tau$ ($n < 0.33/\tau$), the error remains $< 10\%$. Notably, for both approximation formulas, the calculated value for n_0 is lower than the actual value.

For completeness, it should be mentioned that electronics with different dead-time behavior also exist, specifically those where pulses arriving during the dead time do not retrigger it (non-paralyzable behavior). Such electronics can process a new pulse immediately after the dead time has elapsed, regardless of how many pulses arrived during that interval. An example is a detector system where the duration of the analog pulses is negligible compared to the analog-to-digital (AD) conversion time. Pulses arriving during the AD conversion do not interfere with the process, as the analog voltage is typically buffered in a sample-and-hold stage. Although pulses occurring during this conversion window are ignored, the system is ready to process new pulses immediately upon completion of the AD conversion. For this type of dead-time behavior, the maximum achievable output rate approaches a constant value of $n_{max} = 1/\tau$.

In the case of the *ORFEUS* detector, however, the analog pulses are the slowest component in the signal processing chain. Consequently, any optimization of the electronics for future projects should focus on equipping the charge-sensitive amplifiers with faster electronics.

3 Experimental Setup

The experimental setup comprises four components:

- Detector with high-voltage supply and vacuum pump
- Optical bench
- Rack with DPA, pressure gauge, and oscilloscope
- Computer

3.1 Detector with high-voltage supply and vacuum pump

Figure 3.1 shows the detector with its high-voltage (HV) supply. On the left is the vacuum connection leading to the vacuum pump. The vacuum valve mounted on the detector must always be *fully open*, i.e. the valve's actuation screw must be completely unscrewed.

Safety: Always verify the detector valve is fully open *before* enabling high voltage. The pump normally remains on continuously; check the pressure periodically and *disable HV* if it rises above 1×10^{-6} mbar.

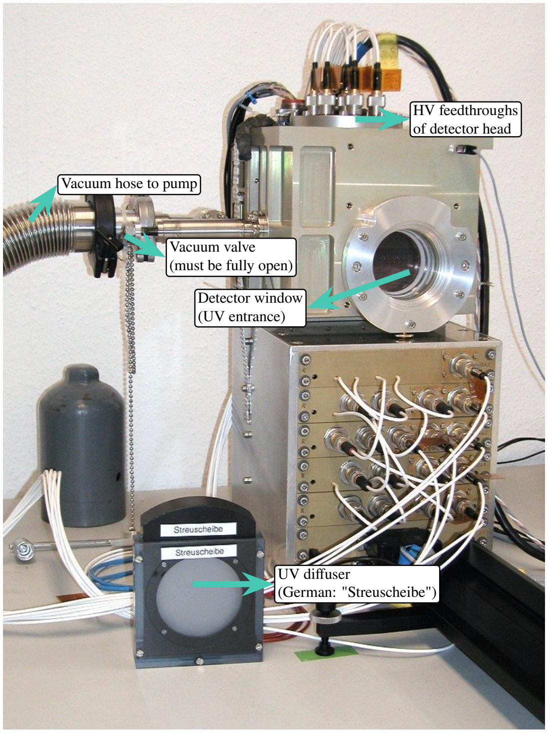

Figure 3.1. Detector head (top) and its high-voltage supply (bottom).

The rack-mounted pressure gauge reads the pressure directly at the pump and displays it in millibar (mbar; numerically equal to hPa). The actual pressure in the detector body is typically about a factor of 100 higher (i.e. worse) than the pump reading because of the limited conductance of the hose and valve. With the detector idle and dark, the pump reading is about 1×10^{-7} mbar to 5×10^{-7} mbar. High voltage may be enabled only if the reading is below 1×10^{-6} mbar.

When HV is switched on, the pressure usually rises temporarily. Under vacuum, internal surfaces (including MCP channel walls) adsorb residual gases. Electron bombardment during operation stimulates desorption (electron-stimulated desorption), briefly increasing the gas load. As the surfaces are "cleaned" with continued operation, the outgassing rate decreases and the pressure returns towards its prior level.

Exercise 7:

Calculate the total inner surface area of all channels of an ORFEUS MCP with a thickness of 1 mm *(see Chap. 2.2.6).*

3.2 Optical Bench

The optical bench (Figure 3.2) comprises the following components:

- Mercury lamp: emits a strong line at 254 nm, within the detector's sensitivity. A UV diffuser is mounted in front of the lamp to homogenise the angular distribution of the emitted light.
- Small iris diaphragm
- Quartz condenser: the irradiance at the detector can be adjusted by varying the distance between the condenser and the lamp.
- Resolution test mask
- Quartz imaging lens with a large iris diaphragm (focal length 20 cm for *visible* light).
- Mask holder with additional test masks

Not all of these components are required for every measurement.

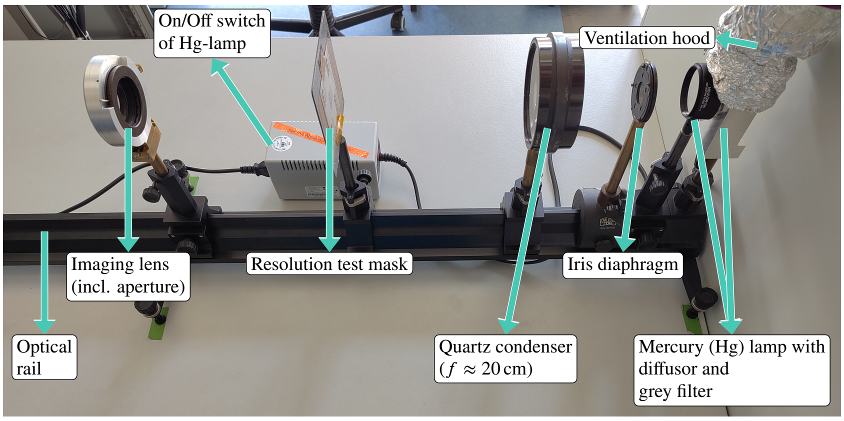

Figure 3.2. Optical bench (example configuration).

Exercise 8:
What is the smallest permissible distance between test mask and detector that still permits imaging with the given lens? What magnification results? Why are the lenses in this experiment made of quartz?

Safety: UV light can irritate the eyes. Avoid viewing the source for extended periods; operate with the diffuser and grey filter mounted. To prevent erythema, do not expose unprotected skin near the lamp for long periods. To limit ozone formation, ensure the ventilation is running. Switch the lamp off when not in use.

3.3 Digital Position Analyzer

The Digital Position Analyzer (DPA) serves as the primary control interface for the detector electronics (see also Chapter 2.4.4). The key front-panel elements are shown in Figure 3.3:

- Pulse counter: Features a selectable integration time (1 s / 10 s).
- Pulse class selector: Determines which events are incremented:
  - Total Pulses: Counts all detected pulses; the trigger threshold is calibrated slightly above the noise floor.
  - Active Pulses: Counts only events processed by the electronics. During an integration, these correspond exactly to the data transferred to the computer.
  - Lower Discriminator: Counts pulses exceeding the lower discriminator threshold.
  - Upper Discriminator: Counts pulses exceeding the upper discriminator threshold.
- Pulses Output: BNC output of the analogue pulses for monitoring via an oscilloscope.
- Oscilloscope Output: Three outputs (X, Y, Z) for a storage monitor to visualize events in real time.
- High Voltage: Power switch for the high-voltage supply unit.
- Detector input: Connector for the detector signal cable.
- Integration stop: Switch to manually terminate an active measurement.
- Mains power: Primary power switch for the DPA unit.
- Integration mode selector:
  - Position 1 (Z): Transmits pulse-height sums (Z) to generate a pulse-height distribution.
  - Position 2 (X, Y): Transmits spatial coordinates to generate an image.
  - Position 3 (X, Y, T): Transmits position and time-of-arrival for time-stamped (list-mode) recording.
  - Position 4 (X, Y, T, Z): Transmits full data sets; required for detector gain mapping.
  - Position 5 (HWI): Reserved; not implemented in the current configuration.
- Integration time display: Shows time in milliseconds with a marker indicating the seconds decimal. The display is *dead-time corrected*; the internal clock increments only when the system is ready to process new events.

- Image-window selector: Defines a sub-region within a 4 × 4 matrix. Sub-images are recorded at 12-bit resolution (1024 × 1024 pixels). Valid X and Y indices range from 0 to 3.

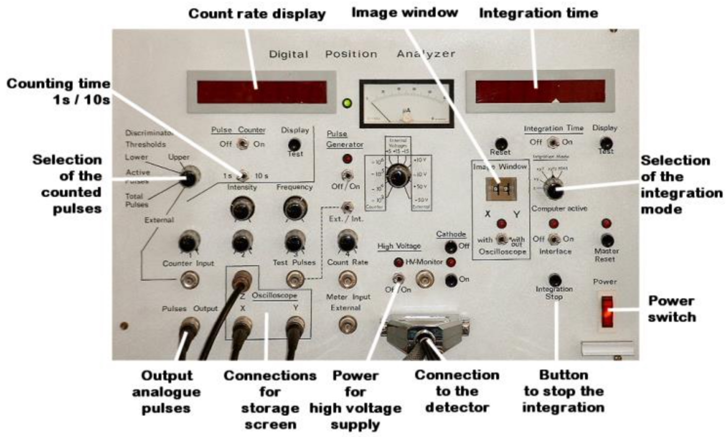

Figure 3.3. Key operating controls of the DPA.

3.4 Storage Screen

An oscilloscope operating in X-Y mode serves as the storage screen (Fig. 3.4) to provide a real-time visualization of the detector image. The DPA provides the necessary X and Y coordinate signals along with a Z-pulse (unblanking) for each registered event. These signals drive the electron beam to a specific coordinate and momentarily increase its intensity, displaying the event as a discrete point of light.

Safety: To prevent permanent phosphor burn-in and extend the lifespan of the device, do not operate the screen in storage mode longer than necessary. Reduce the beam intensity or switch to a non-storage mode if the beam remains stationary or if the event rate is high.

Operational Hints for Students: To achieve optimal image quality, consider the following adjustments:

- **Power button:** Located in the center of the oscilloscope and labeled "Line".
- **Focus:** Adjust to ensure the dots are as small and circular as possible.
- **Persistence:** In storage mode, the persistence control determines how long an event remains visible. Choose a persistence as high as possible, but low enough not to over-saturate the image.

- **Beam Intensity:** Use the beam intensity to set a specific Z-value that must be reached before an X-Y position is displayed. Adjust it just high enough to display real events.
- **Brightness:** With low brightness, the contrast improves, although the overall image brightness is reduced. Typically, a better image is yielded at high persistence and low brightness.

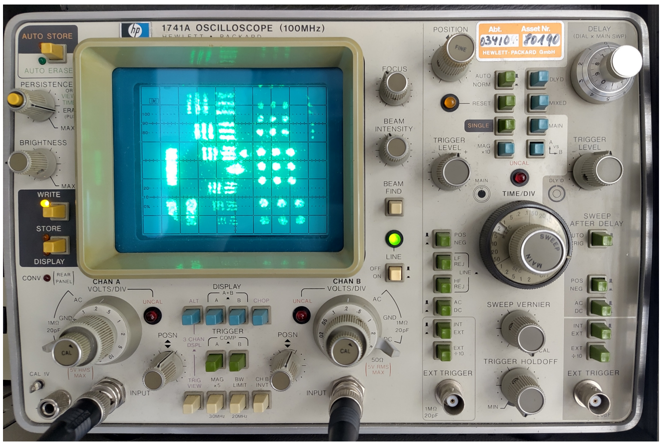

Figure 3.4. Storage screen displaying the real-time spatial distribution of registered events.

3.5 Oscilloscope

The oscilloscope (Fig. 3.5), an *Agilent InfiniiVision MSO7104B*, is used to monitor the analog pulses from the detector. To display test pulses, the following initial settings are recommended:

- Vertical Scale: 1 V/div
- Horizontal Scale: 0.5 μs/div
- Trigger: Edge trigger, rising edge, sufficiently large positive threshold to display only one pulse

When displaying test pulses, an inverted (negative) pulse is often visible alongside the primary signal. This occurs because the test generator produces square-wave pulses. Both the rising and falling edges of the square wave produce signals. Only the falling edge simulates the negative charge collection on the anode.

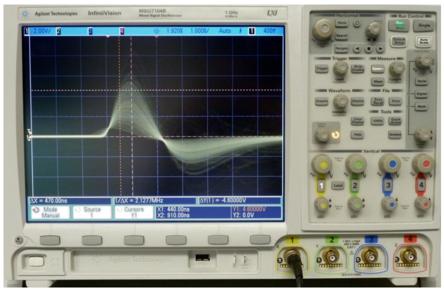

Figure 3.5. Oscilloscope displaying typical detector sum pulses.

3.6 Computer and Software

Two software applications are required for detector operation and data acquisition. The program *Detector-Control* manages the high-voltage (HV) supply, controls test pulses and provides a gain display. The program *Datenerfassung* (only German version available) is used for data collection and allows for image integration of events registered by the detector. Both programs are briefly introduced below.

3.6.1 Program *Detector-Control*

The *Detector-Control* software is primarily used to control and monitor the detector's high-voltage supply. As a critical safety feature, it monitors the vacuum system pressure and will automatically shut down the HV, or prevent it from being activated, should the pressure exceed a predefined safety threshold (maximum 10^{-6} mbar).
The main functions and displays are described below. The program configuration (*Main menu* → *Setup*) is already optimized for the experiment; only the protocol update rate should be adjusted when needed during an experiment. All measured parameters are logged periodically to a protocol (log) file on the hard disk.

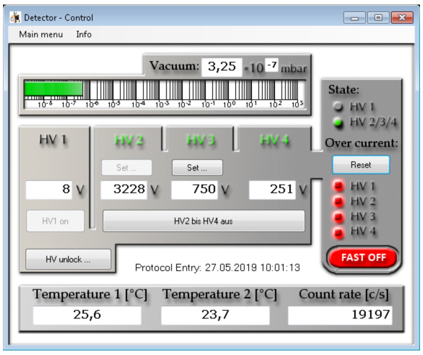

Figure 3.6. Main interface of the *Detector-Control* program.

Main Window

The main window shows the pressure of the vacuum system, the four measured voltages of the high-voltage supply, and the detection of an overcurrent in any of the four high-voltage modules. Two temperature values are also displayed (outside the detector housing and at the charge amplifiers), as well as the current count rate and the timestamp of the last protocol entry.

The high voltage is switched on by clicking the buttons labelled *HV1 on* and *HV2 to HV4 on*. Before these buttons can be activated, they must be unlocked by clicking the button labelled *HV unlock ...* . You then have to confirm that the vacuum valve of the detector is open (only then is the measured pressure valid for the detector) by selecting the option "*Vacuum valve is open!*". After confirming this, the button "*HV2 to HV4 on*" is enabled for five seconds. Only during this time is it possible to switch on the high voltage. This prevents an unintended switching on, which could have catastrophic consequences.

Test Pulses

The *Test Pulses* menu item activates the internal test pulse generator (see Section 2.3.3). This interface allows the user to modify the pulse frequency, the switching interval between pulse types, and the selection of the six available pulse types. Since only one test pulse type can be active at a time, the selected types are cycled in sequence according to the specified switching rate.
If test pulses are intended to be active during image integration, a frequency of 1 Hz or 10 Hz is recommended. When selecting a 1 Hz frequency, the switching rate should be increased to 10 seconds.

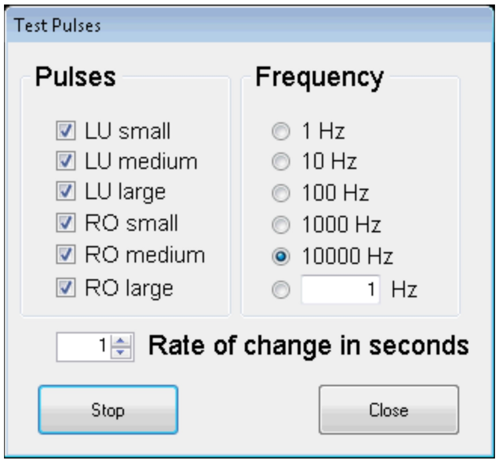

Figure 3.7. The *Test Pulses* configuration window in the *Detector-Control* program.

Test Pulse Display

The *Test Pulse Display* window provides averaged X, Y, and Z values calculated from 1,000 pulses of the currently active test pulse type. The software also computes the standard deviation σ, which is multiplied by a factor of $c = 2.35$ and displayed as DX, DY, and DZ. These values represent the Full Width at Half Maximum (FWHM) of the point spread function (refer to Eq. 2.5.2). While X and Y are provided in pixel units, the pulse height Z is converted to Volts for consistency with the oscilloscope display.

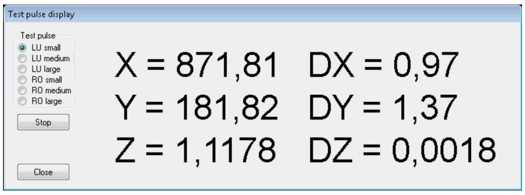

Figure 3.8. The *Test Pulse Display* diagnostic window in the *Detector-Control* program.

Safety: Ensure that the high voltage is switched off when using this display. Even low levels of MCP dark events will significantly distort the statistical evaluation of the test pulses.

Test Pulse Check

The *Test Pulse Check* feature performs the same statistical evaluation as the *Test Pulse Display*, but it automatically iterates through all six test pulse types sequentially and presents the results in a tabular format. The row corresponding to the currently active test pulse is highlighted in yellow, allowing the user to track real-time changes across the different pulse types.

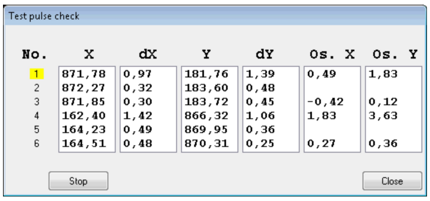
Test pulse check

No.	X	dX	Y	dY	Os. X	Os. Y
1	871,78	0,97	181,76	1,39	0,49	1,83
2	872,27	0,32	183,60	0,48		
3	871,85	0,30	183,72	0,45	-0,42	0,12
4	162,40	1,42	866,32	1,06	1,83	3,63
5	164,23	0,49	869,95	0,36		
6	164,51	0,48	870,31	0,25	0,27	0,36

Stop Close

Figure 3.9. The *Test Pulse Check* diagnostic table in the *Detector-Control* program.

Additionally, the columns *Os. X* and *Os. Y* show the differences between successive X and Y values: Os. X(1) $= X(2) - X(1)$, Os. X(3) $= X(3) - X(2)$, and similarly for $X(4) \dots X(6)$ and the corresponding Y values. This highlights pulse-height-dependent variations, which are typically caused by electronic offset errors (refer to Chapter 2.5.4).

Safety: As with the *Test Pulse Display*, it is critical that the high voltage is switched off during this check to ensure dark counts do not skew the statistical results.

This diagnostic tool was originally developed for the ground station software used during the second *ORFEUS* flight. It allowed for rapid functional verification of the entire detector electronics in the field. Specifically, it enabled the team to verify that the electronic resolution remained consistent with pre-flight laboratory measurements.

Gain Display

The *Gain Display* shows the mean value of the Z-coordinate based on at least 1,000 measurements (at count rates exceeding 1,000 s^{-1}, the integration time is at least one second). The gain is converted into volts, corresponding to the summed pulse signal observed on the oscilloscope.
A measure for the distribution width is calculated by multiplying the standard deviation by a factor of $c = 2.35$; this value is displayed as a percentage of the mean gain.

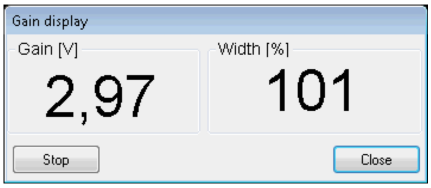

Figure 3.10. The *Gain Display* window within the *Detector-Control* program.

Only in the case of a perfect Gaussian distribution would this calculated value correspond exactly to the geometric Full Width at Half Maximum (FWHM). For actual pulse-height distributions, this value serves only as an empirical approximation of the FWHM. This display is primarily utilized to adjust the high-voltage *HV3* (see Fig. 3.6), which is used to regulate the detector gain.

3.6.2 *Data Acquisition* Program

The *Acquisition* program is used for the collection and spatial/temporal integration of detector data. The primary menu item *Data* (see Fig. 3.11) provides access to various integration routines. The numbers shown in parentheses in the software menu correspond to the required physical positions of the integration mode selector on the DPA front panel (refer to Section 3.3 and Fig. 3.3). If the DPA selector is not set correctly, the corresponding menu items in the software will be grayed out and disabled.

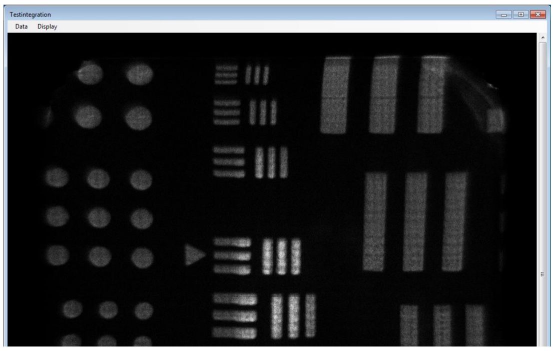

Figure 3.11. Interface of the *Acquisition* program during an active image integration.

Menu item *Image Integration*

Selecting the menu item *Image Integration* initiates the integration of a spatial image with a resolution of 1024×1024 pixels. The integrated image is refreshed every 10 seconds in the main display window (Fig. 3.11).
During active integration, the menu bar only displays the entries *Data* and *Display*. Specific sub-items allow the user to modify the image presentation on the screen (Fig. 3.12). Integration can be terminated using the physical *Integration Stop* button on the DPA (Fig. 3.3) or the corresponding stop command under the *Data* menu.

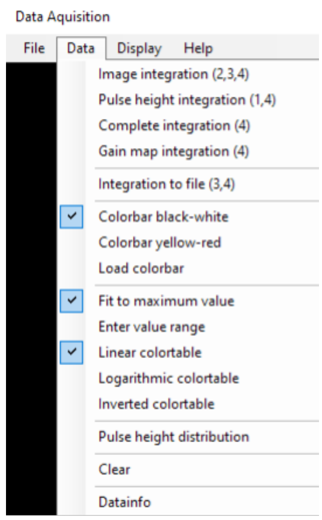

Figure 3.12. The *Data* menu of the *Acquisition* program.

Menu item *Pulse height integration*

Selecting *Impulshöhe integrieren* starts the integration of a pulse-height distribution. The resulting histogram is displayed in a separate window (Fig. 3.13) and is updated every 10 seconds. This window can be resized manually to suit the user's requirements. Both linear and double-logarithmic axis layouts are available for selection.

Menu item *Complete integration*

Menu item *Complete integration* starts the integration of an image and a pulse height distribution at the same time.

Menu item *Gain Map Integration*

Selecting the menu item *Gain Map Integration* initiates the generation of a gain map. In this mode, the intensity of each pixel represents the mean pulse height at that specific coordinate. The software utilizes three internal image buffers for this calculation:

1. The first integrates a standard photon image (count rate).
2. The second accumulates the sum of the Z-coordinates for every registered event.
3. The third calculates the ratio of the pulse-height sum to the total number of photons per pixel.

This process effectively maps the averaged MCP gain across the entire active detector area. The display can be toggled between the gain map and the standard photon image.

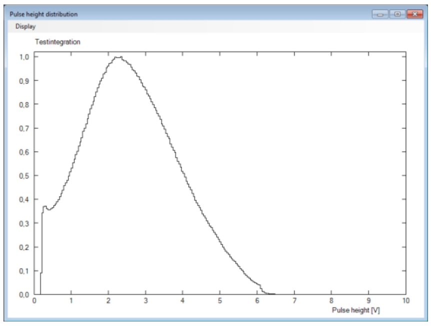

Figure 3.13. The pulse-height distribution window during integration (linear axes). X: pulse height [V]; Y: relative occurrence.

3.6.3 Program *Pressure Center One*

The program *Pressure Center One* records data from the *Center One* pressure gauge and the sputter ion pump via a serial interface. Typically, the software samples these values every minute. If the *Fast readout* option is enabled, the sampling interval is reduced to five seconds. The *Clear protocol* button erases the current log file and initializes a new one.

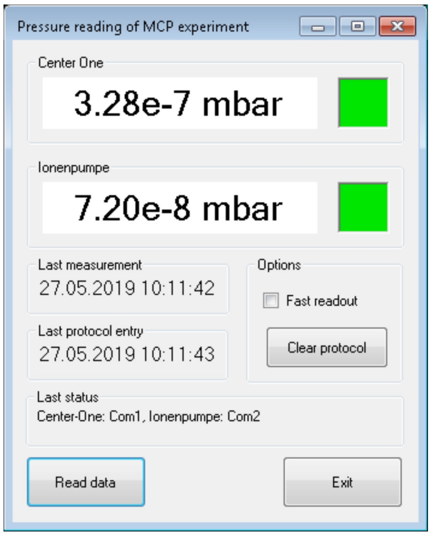

Figure 3.14. Interface of the *Pressure Center One* monitoring program.

4 Experimental Procedure

4.1 Introductory Notes

During the experimental procedure, you must record your measurements and observations such that the course of the experiment remains fully reconstructible, both for you and the laboratory supervisor, at a later date. Consequently, your notes should be labeled with the corresponding section and exercise numbers from these instructions.

Before commencing the experiment, ensure you have read the document *"Guidelines for the Lab Course."* Always remember to record every measured value with its appropriate physical unit. **The original raw records must be attached to the final lab report (protocol).**

Safety: Do not touch the optical lenses with your fingers! Skin oils can contaminate and permanently damage high-precision optical coatings.

4.2 System Start-up

Follow the start-up procedure strictly in the order given below:

Safety: The high-voltage supply must only be operated if the vacuum pressure is below 10^{-6} mbar. Confirm that the detector valve is fully open (screw unscrewed to the stop position, approximately 14 mm) to ensure the pressure gauge accurately reflects the vacuum level within the detector housing.

- **DPA:** Switch on the Digital Position Analyzer.
- **Computer:** Power on the PC and log in.
- **Software:** Ensure any German software instances are closed. Launch the English versions of *Detector-Control* and *Pressure Center One*.
- **HV Unit:** Switch on the power supply for the high-voltage unit via the toggle on the DPA (see Fig. 3.3).
- **Oscilloscope:** Power on the device (switch located at the bottom left).
- **Storage Screen:** Power on using the "Line" button in the center. Select a low persistence setting unless high persistence is explicitly required for your measurement.
- **Detector-Control:** Click the *Reset* button in the *Overcurrent* box.
- **Detector-Control:** Select *Delete protocol file...* to initialize a new log. Under *Setup*, set the *Update Rate* in the *Protocol Settings* panel to 60 s.
- **Pressure Center One:** Click *Clear protocol* to reset the pressure log.
- **DPA:** Press the *Master Reset* button.
- **UV Lamp:** If applicable, activate the suction device for the UV lamp.

4.3 Test Pulses

Begin with an electronics checkout. In the *Detector-Control* program, select the menu item *Test Pulses* and activate the generator. On the oscilloscope screen, you should observe test pulses that vary in height every second. On the storage screen (increase persistence), the test pulse should shift its position between opposite corners every three seconds.

Measure the peak amplitude of the test pulses by selecting only one pulse type at a time in the *Test Pulses* window. Record the maximum voltage values for all six test pulse types. Afterward, stop the generator and close the *Test Pulses* window. Open the *Testpulse Display* menu item and record the Z value (displayed in Volts) for each type. Once complete, stop the pulses and close the window.

Exercise 9:

Compile your measured peak voltages and the corresponding software Z values for all test pulse types into a table. How well do your manual measurements agree with the Z values displayed by the software? Calculate the absolute differences and the percentage deviations between your measurements and the provided Z values.

Next, select the menu item *Testpulse Check* and start the sequence. After at least two full cycles, capture a screenshot of the *Testpulse Check* window using the *Snipping Tool*: click the camera icon, then right-click within the *Test Pulse Check* window (ensure that the capture mode is set to "Window" via *File / Import / Snapshot / Setup...* beforehand).

Exercise 10:

Include the screenshot of the Test Pulse Check table in your report. Recapitulate and compare the three methods used in this section to determine the pulse height (Z value). Describe how the Z values are determined in each case and discuss the advantages and disadvantages of each method.

4.4 High-Voltage Activation

Prepare the optical bench by removing all components except for the lamp (with the diffuser disk), the gray filter positioned immediately adjacent to it, and the condenser. Position the condenser approximately 50 cm in front of the lamp.

Safety: Do not touch any optical components with your fingers.

In the *Detector-Control* program, click *HV unlock ...*. Ensure the detector valve is open, then select the option *Vacuum valve is open!* and click **OK**. **Within a five-second window**, click the *HV2 to HV4 on* button (note that *HV1* remains off). The high voltage is now active, and the detector should begin producing pulses.[7] Set the count rate selector switch on the DPA to the *Total Pulses* position.

Next, switch on the UV lamp and increase the persistence on the storage screen.

[7] If not, the supervisor will adjust *HV2* to an appropriate initial value.

Safety: The UV lamp must only be operated while the suction/exhaust device is active to prevent the accumulation of ozone.

It typically takes one to two minutes for the lamp to reach full intensity, during which time the count rate will steadily increase. Adjust the position of the condenser until the count rate stabilizes at approximately 10,000 s^{-1}.

In the *Detector-Control* program, open the *Gain Display*. Click the **Set...** button below the *HV3* indicator and adjust the voltage in 10 V increments until a mean gain of 3.0 V is achieved. Record this final high-voltage value in your notes; you must update this record whenever the gain settings are modified. Once the gain is stabilized, close the HV3 setup window and exit the *Gain Display*.

4.5 Dark Count Rate

Switch off the UV lamp and close the detector entrance window by inserting the light-tight blind into the slot at the detector entrance. Set the counting interval on the DPA counter to 10 s.

Record ten consecutive counter values and calculate their arithmetic mean to determine the average dark count rate.

Note: A counter reading is valid only when the green LED to the right of the DPA display is illuminated. The value remains visible for only one second before the next gate interval begins.

4.6 Pulse Height Distribution

4.6.1 Full-Field Measurement

Reactivate the UV lamp and open the *Gain Display* window. Adjust *HV3* until the mean gain reaches 3.0 V. Record the gain and width values **before and after** the pulse-height integrations. Ensure the *Gain Display* is closed during the integration process. Set the DPA integration mode selector to *position 4 (x, y, t, z)*.

Note: You must reset the DPA time counter prior to every new integration.
In the *Acquisition* program, initiate a pulse-height integration (refer to Section 3.6.1). Terminate the integration once the distribution curve is sufficiently smooth (typically after $\approx$ 200 s). Save the resulting plot via *Display → Save bitmap*. Do not forget to perform the second gain measurement immediately after stopping the integration.

4.6.2 Partial-Field Measurement

Define a partial image window on the DPA (*Image Window:* $X = 2, Y = 0$) and repeat the pulse-height integration procedure. As before, record the gain and width **before and after** the measurement and save the resulting bitmap. Upon completion, reset the image window to the full-field setting ($X = 9, Y = 9$).

Exercise 11:

Use the pulse-height distribution plots to estimate the peak position (maximum) and the geometric FWHM. Annotate these quantities directly on your plots. Use your own method to convert the spatial dimensions measured in the plot to a voltage. Express the FWHM as a percentage of the peak position.

Identify the physical reasons for the observed differences in peak position and FWHM between the full-field and partial-field measurements. Compare your graphically estimated values for gain and width with those recorded from the software's Gain Display (use the average of the measurements taken before and after integration). Why do the software-calculated values differ from your graphically estimated values? Explain the mathematical algorithm used by the software to calculate gain and width.

4.7 Outgassing

In the *Detector-Control* program, select the *Setup* menu item and adjust the protocol update rate to 5 s. Simultaneously, enable the *Fast Readout* option in the *Pressure Center One* program. Open the *Gain Display* and adjust *HV3* until a mean gain of 3.0 V is reached.

Keep the Gain Display active throughout this measurement to ensure that the gain values are automatically recorded in the protocol log.

Slowly move the condenser toward the lamp until a total count rate of 50,000 s^{-1} is achieved. Maintain this rate for five minutes, then adjust the condenser to return the count rate to 10,000 s^{-1}. Wait for another five minutes before concluding (you may begin work on Exercise 13 in the meanwhile). **Finally, reset the update rate to 60 s** in both *Detector-Control* and *Pressure Center One*, then close the *Gain Display*.

After the experiment, locate the semicolon-separated log file at `C:\Protocol\HV\mcp_protokoll_lang.txt` and copy it to your personal working directory.

As the file contains no header row, use the following table to identify the data columns:

Col.	Parameter	Description
1	Timestamp	Date and time of the measurement entry.
2	MCP Pressure	Vacuum pressure in the detector housing [mbar].
3	Preamp Temp	Temperature at the charge-sensitive amplifiers [°C].
4	Housing Temp	Temperature outside the detector housing [°C].
5	Count Rate	Total detected events per second [s^{-1}].
6–7	(Internal)	Internal system flags.
8	HV1 (Grid)	Voltage applied to the entry grid [V].
9–11	HV2 – HV4	Voltage applied to the MCP stages [V].
12	Mean Gain	The calculated average pulse height [V].
13	Width	The width of the pulse-height distribution [%].

The directory `C:\MCP\Lab-course\mcp-lab-course-analysis\` contains Python scripts designed for data analysis in this and subsequent experiments. Identify the start and end times of your specific measurement window within the log file. To generate the required plot, update the `plot_protocol_outgassing.py` script (or your own custom script) with these timestamps and the correct path to your data folder.

> **Exercise 12:**
> *Plot the chronological progression of both the gain and the vacuum pressure in a single diagram and include it in your report. Comment on the results: Why does the pressure increase at high count rates? Why does the gain decrease accordingly? Describe the behavior of both parameters when the count rate is reduced back to 10,000* s^{-1}.

4.8 Flat-field and Gain Map Integration

Remove the large diffuser from the protective housing and mount it directly in front of the detector window. Adjust the count rate to approximately 20,000 s^{-1} and ensure the gain is set to 3.0 V. Initiate a *Gain Map Integration* (refer to Section 3.6.1). Enter the required integration parameters in the start-up window and specify a unique filename for the data set.

The integration should proceed until a Signal-to-Noise Ratio (SNR) of 10 is achieved for the exposed regions of the image. Due to the significant time required, it is recommended to perform this measurement during a scheduled break or lunch period.

> **Exercise 13:**
> *Determine the number of counts required per pixel to achieve an SNR of 10. Based on this, calculate the necessary total integration time using the Active Pulses rate (assume an area of approximately* 900×900 *exposed pixels). Use the provided Python analysis tool (`plot_flat-field.py`) to generate printouts of the resulting images.*

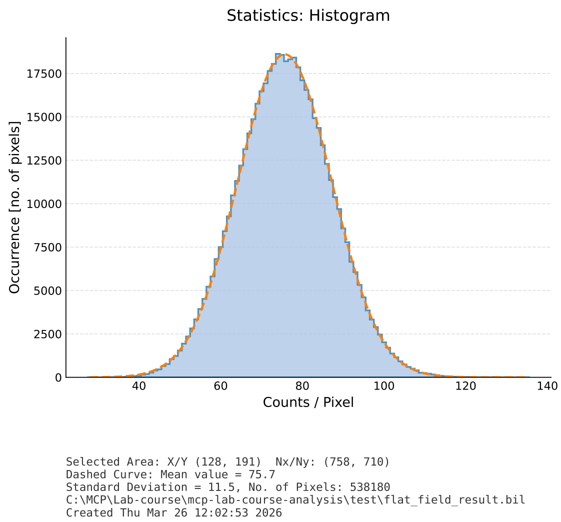

Figure 4.1. Histogram of the intensity distribution for a selected image section. The dashed curve represents a Gaussian fit to this data.

Evaluation of Homogeneity

This analysis may be performed after all experimental data has been collected.

Evaluate the small-scale homogeneity of the flat-field image. To do this, generate a histogram of an image section that appears spatially homogeneous (using `Homogeneity.py`). Include this histogram in your protocol. If the pixel-to-pixel intensity variations were purely statistical (stochastic), the histogram would follow a Poisson distribution. Since the mean value is large ($\mu \approx 100$), the Poisson distribution can be accurately approximated by a Gaussian distribution with a standard deviation of $\sigma = \sqrt{\mu}$. As observed in the sample data, the theoretical curve may not perfectly coincide with the measured histogram. This indicates that intensity variations are not solely statistical but include systematic errors, suggesting that the detector homogeneity is not perfectly optimized. Figure 4.1 displays a sample histogram. The dashed curve represents a Gaussian distribution with an identical mean value.

> **Exercise 14:**
> *Assess the homogeneity of your selected image section by comparing the measured histogram with the theoretical Gaussian distribution. Provide the* ***exact, complete formula*** *for the dashed Gaussian curve shown on your printout. This formula contains three parameters that must be estimated from the numerical data on your plot. Verify your formula by calculating two specific points—one on the slope and one near the maximum—and mark these on your printout. Justify your choice for the three parameters (A, μ, and σ).*

4.9 Determination of the Focal Length by the Bessel Method

Remove the diffusion disk located in front of the detector and arrange the optical components on the optical bench as follows:

- Lamp with double diffusion disk; small iris diaphragm positioned as close as possible in front of the lamp.
- Test mask, placed approximately 90 cm from the front of the detector housing.
- Condenser, positioned 20 cm from the small iris diaphragm.
- Imaging quartz lens (iris diameter 35 mm) between the detector and the test mask, positioned closer to the test mask.

The Bessel method for determining the focal length requires the object-to-image distance e to be strictly greater than four times the focal length ($e > 4f$). Under this condition, there are exactly two distinct lens positions that produce a sharp image. By measuring the physical displacement d between these two positions, the focal length f of a thin lens can be calculated using the following equation (Bergmann/Schäfer, 1962 [2]):

$$f = \frac{e^2 - d^2}{4e} \tag{4.9.1}$$

First, determine the object-to-image distance e between the test mask and the MCP surface. Measure the physical distance between the test mask and the front face of the detector housing (greenish-golden surface) with an accuracy of 1 mm. Next, account for the distance from the housing face to the MCP surface. The mechanical distance is 26.7 mm, but the 5 mm thick quartz entrance window ($n = 1.5$ at $\lambda = 254$ nm) alters the optical path. The apparent thickness of the window is $5\,\text{mm}/1.5 \approx 3.3$ mm, which results in an optical shortening of 1.7 mm. Therefore, the effective distance is $26.7\,\text{mm} - 1.7\,\text{mm} = 25.0\,\text{mm}$. **To find e, add 25 mm to your measured test mask-to-housing distance.**

Next, locate the two optimal lens positions that produce a sharp image. Begin with the position closer to the test mask. Focus the image initially by observing the real-time display on the storage screen. Adjust the count rate to approximately 10,000 s^{-1} using the small iris diaphragm.

Start an image integration for a fixed duration (e.g., 100 s). Export the bitmap and open it; it will be used for comparison with the next image.

Move the lens by 2 mm, recording its position on the optical bench scale (consistently use the edge of the slider facing the lamp as your reference). Integrate for the same duration and export the bitmap. Compare the sharpness of the two images to determine the correct direction for subsequent adjustments. Iterate this process until you find the optimal focal position to an accuracy of 1 mm.

Now, find the second sharp imaging position (close to the detector). Adjust the count rate to 3,000 s^{-1} and repeat the procedure described above. The absolute difference between these two optimal slider positions yields your value d.

Additionally, determine the focal length of the lens for *visible* light by imaging a distant object onto a screen.

> **Exercise 15:**
> *Calculate the focal length of the quartz lens for a wavelength of 254 nm using Eq. 4.9.1. Compare this result to the focal length measured with visible light. What is the physical reason for this difference?*

4.10 Dead Time and Efficiency

Move the condenser until a count rate (*Total Pulses*) of approximately 100,000 s^{-1} is achieved. The vacuum pressure must not exceed 1×10^{-6} to 2×10^{-6} mbar; otherwise, the automatic pressure monitor will shut down the high voltage!

Record the counter values for *Total Pulses*, *Active Pulses*, and both discriminator thresholds. Reduce the count rate (*Total Pulses*) in steps of 10,000 s^{-1} by moving the condenser away from the lamp. At each step, record all four counter values (ensure you also include an additional measurement at 75,000 s^{-1}).

Important:
During the read-out of the counter values for the *Active Pulses*, the *Gain Display* must **not** be active!

Exercise 16:

Create an Excel table (or use a Python script) for your measured values. Calculate a dead time correction for "Total Pulses" and "Lower Threshold" according to Eq. 2.5.23, assuming a counter dead time of 2 μs. Calculate the measured efficiency using the following relation:

$$\text{Efficiency} = \frac{\text{Active Pulses}}{\text{Lower Threshold} - \text{Upper Threshold}}$$

Calculate the theoretical values for the efficiency according to Eq. 2.5.21 (see Fig. 2.15) and present both the theoretical and measured values in a single diagram. Treat the detector dead time as a free parameter (stored in a separate variable or table cell). Adjust this dead time value until the theoretical curve optimally fits your measured data.

Determine n_{max} for this specific dead time using Eq. 2.5.22. Compare this calculated n_{max} with your actual maximum measured value for Active Pulses.

5 Literature and Sources

[1] J. Barnstedt, W. Gringel, N. Kappelmann and M. Grewing. 'The ORFEUS II Echelle spectrum of HD 93521: A reference for interstellar molecular hydrogen'. In: *Astronomy and Astrophysics Supplement Series* 143.2 (Apr. 2000), pp. 193–210. DOI: 10.1051/aas:2000176. URL: https://doi.org/10.1051%2Faas%3A2000176.

[2] L. Bergmann and C.Schaefer. *Lehrbuch der Experimentalphysik*. Vol. 3. Walter de Gruyter and Co., 1962. Chap. I. (Wellenoptik). DOI: 10.1515/9783111500737. URL: https://doi.org/10.1515/9783111500737.

[3] C. A. Craven et al. 'Recent Advances in Large Area Micro-channel Plates and LAPPD™'. In: *Proceedings of International Conference on Technology and Instrumentation in Particle Physics 2017*. Ed. by Z.-A. Liu. Singapore: Springer Singapore, 2018, pp. 319–324. ISBN: 978-981-13-1316-5.

[4] S. Diebold. 'Proportional Counters and Microchannel Plates'. In: *Handbook of X-ray and Gamma-ray Astrophysics*. Ed. by C. Bambi and A. Santangelo. Singapore: Springer Nature Singapore, 2022, pp. 1–36. ISBN: 978-981-16-4544-0. DOI: 10.1007/978-981-16-4544-0_16-1. URL: https://doi.org/10.1007/978-981-16-4544-0_16-1.

[5] G. W. Fraser. *X-ray Detectors in Astronomy*. Cambridge Astrophysics. Cambridge University Press, 1989. Chap. 3: Microchannel Plates, p. 116. DOI: 10.1017/CBO9780511735554. URL: https://doi.org/10.1017/CBO9780511735554.

[6] G. Knapp. 'Crossed grid anode and its image partitioning'. In: *Review of Scientific Instruments* 49.7 (July 1978), pp. 982–987. ISSN: 0034-6748. DOI: 10.1063/1.1135513. eprint: https://pubs.aip.org/aip/rsi/article-pdf/49/7/982/19166754/982_1_online.pdf. URL: https://doi.org/10.1063/1.1135513.

[7] C. Martin, P. Jelinsky, M. Lampto, R. F. Malina and H. O. Anger. 'WEDGE-AND-STRIP ANODES FOR CENTROID-FINDING POSITION-SENSITIVE PHOTOM AND PARTICLE DETECTORS'. In: *Review of Scientific Instruments* 52.7 (Feb. 1981). ISSN: 0034-6748. DOI: 10.1063/1.1136710. URL: https://www.osti.gov/biblio/993752.

[8] U. Tietze and C.Schenk. *Halbleiter-Schaltungstechnik*. Vol. 10. Springer Berlin, Heidelberg, 1993. DOI: 10.1007/978-3-662-07639-2. URL: https://doi.org/10.1007/978-3-662-07639-2.

[9] A. S. Tremsin and O. H. W. Siegmund. 'The quantum efficiency and stability of UV and soft x-ray photocathodes'. In: *Ultrafast X-Ray Detectors, High-Speed Imaging, and Applications*. Ed. by Z. Chang, J.-C. Kieffer, J. B. Hastings, S. Kleinfelder and D. L. Paisley. Vol. 5920. International Society for Optics and Photonics. SPIE, 2005, p. 59200I. DOI: 10.1117/12.621761. URL: https://doi.org/10.1117/12.621761.

[10] P. Weinzierl and M. Drosg. *Lehrbuch der Nuklearelektronik*. Vol. 1. Springer Vienna, 1970. DOI: 10.1007/978-3-7091-5109-9. URL: https://doi.org/10.1007/978-3-7091-5109-9.

6 Appendix: Natural Constants

Quantity	**Symbol**	**Value**	**Unit**
Speed of light in vacuum	c	2.99792458×10^{8}	m/s
Elementary charge	e	$1.60217663 \times 10^{-19}$	C
Planck constant	h	$6.62607015 \times 10^{-34}$	$J \cdot s$
		$4.13566770 \times 10^{-15}$	$eV \cdot s$
Vacuum permittivity	ϵ_0	$8.854187813 \times 10^{-12}$	$A \cdot s/(V \cdot m)$